Coupling vegetation organization patterns to soil resource heterogeneity in a central Kenyan dryland using geophysical imagery

Trenton E. Franz,[1] Elizabeth G. King,[2] Kelly K. Caylor,[1]
and David A. Robinson[3]

Received 15 October 2010; revised 14 April 2011; accepted 1 June 2011; published 30 July 2011.

[1] In dryland ecosystems, understanding the effects of heterogeneity in soil moisture and geophysical properties on vegetation structure and dynamics poses a suite of challenging research questions. Heterogeneity in soil depth can affect resource availability and the subsequent organization of woody vegetation, while spatiotemporal variation in soil moisture can reveal important ecohydrological feedbacks that govern the outcome of anthropogenic activities on the organization of dryland vegetation. In this research we investigate two cases of soil resource heterogeneity that affect the organization of dryland vegetation patterns by expanding previous electromagnetic induction (EMI) imaging techniques. In the first case we examine the influence of soil depth as a control on soil resource availability on hillslopes in tree-grass systems in central Kenya. Our results indicate that woody vegetation clumping occurs where soil depth changes, and the deeper rooted *Acacia tortilis* occurs on deep soils while the drought tolerant *Acacia etbaica* occurs on shallow soils. In the second case we examine daily patch–interpatch scale moisture dynamics following two different-sized rain events in a degraded landscape. With the aid of a numerical subsurface flow model, EMI, and soil moisture data, we have identified a possible positive feedback mechanism (''soil moisture halo effect'') that we believe may have contributed to the proliferation and two-phase pattern formation of a native succulent *Sansevieria volkensii* in degraded ecosystems of Kenya. By determining how different plants respond to, and modify, the soil environment, we can better understand resource capture and dynamics, which in the longterm will help to develop management strategies.

Citation: Franz, T. E., E. G. King, K. K Caylor, and D. A. Robinson (2011), Coupling vegetation organization patterns to soil resource heterogeneity in a central Kenyan dryland using geophysical imagery, *Water Resour. Res., 47*, W07531, doi:10.1029/2010WR010127.

1. Introduction

[2] Savanna ecosystems, characterized by the codominance of trees and grasses, continue to intrigue scientists in terms of the factors that control their structure and spatial pattern development [*Asbjornsen et al.*, 2011; *Bond*, 2008; *Higgins et al.*, 2007; *Sankaran et al.*, 2005, 2008; *Scholes and Archer*, 1997; *Tietjen et al.*, 2010]. Rainfall arriving at the soil surface is partitioned between infiltration and runoff. The spatial distribution of soil texture and topography are physical factors that influence the partitioning and resulting soil moisture distribution patterns. Biotic factors also control soil resource heterogeneity and resource cascades through the landscape. Soil animal communities, such as ants and termites, affect vegetation structure and composition by modifying the subsurface soil characteristics (i.e., porosity, texture, and infiltration rates) [*Brody et al.*, 2010; *Darlington*, 2005; *Fox-Dobbs et al.*, 2010; *Pringle et al.*, 2010] and above-ground vegetation structure through complex interactions with herbivores [*Palmer*, 2003]. In addition, individual plants and vegetation patches modify the soil environment [*Belsky et al.*, 1989], changing the partitioning between runoff and infiltration due to the presence of soil biotic crusts, obstruction of surface flow, preferential flow paths along stems and roots, and higher soil organic matter [*Belnap and Gillette*, 1998; *Belsky et al.*, 1989]. Identifying hydrological, ecological, and pedological mechanisms that determine soil resource patterns [*Lin et al.*, 2006], and understanding which mechanisms are dominant in which areas and at what scales, will help ascertain the appropriate ecohydrological models for understanding system behavior [*Borgogno et al.*, 2009; *Kefi et al.*, 2007; *Rietkerk et al.*, 2002]. Furthermore, developing robust models that can incorporate such mechanisms to accurately predict system response to perturbations is critical for developing management restoration strategies in the longterm [*Ludwig et al.*, 2005; *Rietkerk et al.*, 2004; *Scheffer et al.*, 2009; *Turnbull et al.*, 2008].

[3] A major impediment to identifying different hydrological, ecological, and pedological mechanisms is a lack of observational soil moisture data to test, either qualitatively or quantitatively, hydrological model development [*Vereecken et al.*, 2008]. Soil moisture sensors can provide high temporal resolution data but have small support volumes

[1]Department of Civil and Environmental Engineering, Princeton University, Princeton, New Jersey, USA.
[2]Department of Ecology and Evolutionary Biology, Princeton University, Princeton, New Jersey, USA.
[3]Centre for Ecology and Hydrology, Environment Centre Wales, Bangor, UK.

0043-1397/11/2010WR010127

and lack spatially explicit coverage for understanding vegetation patch–interpatch dynamics [*Robinson et al.*, 2008b]. Quantifying the vertical and horizontal heterogeneity in plant available water is essential for understanding intercanopy–canopy vegetation dynamics [*Breshears et al.*, 2009]. A combination of soil moisture sensing and noninvasive geophysical imaging [*Hinnell et al.*, 2010] may provide a better spatiotemporal view of soil moisture dynamics toward understanding processes at the patch–interpatch scale. Research that enhances the spatiotemporal scope of soil moisture measurements, and couples that with geophysical properties and vegetation organization, will greatly advance our understanding of landscape ecohydrological functioning. In this study, we sought to couple enhanced soil moisture quantification with measurements of geophysical and vegetation attributes to gain new insight into dryland biophysical function (Figure 1).

[4] Electromagnetic induction (EMI) is proving to be a useful tool for understanding soil spatial heterogeneity [*Abdu et al.*, 2008; *Robinson et al.*, 2008a]. Widely used for determining soil salinity and texture, EMI has been exploited by hydrologists to provide spatial information regarding soil water distribution [*Kachanoski and Dejong*, 1988; *Robinson et al.*, 2009; *Sheets and Hendrickx*, 1995]. The instrument works by transmitting a magnetic field, which induces electrical current loops in the soil and produces secondary magnetic fields, which are received by the instrument. The ratio of the primary and secondary magnetic fields is proportional to the bulk electrical conductivity at low induction numbers [*Abdu et al.*, 2007; *Sherlock and McDonnell*, 2003]. The instrument produces an integrated average measurement over a penetration depth that depends on the sensor coil spacing and carrying height. For example, a 1 m coil spacing will give a penetration depth (70% of signal sensitivity) of ~1.5 m in the vertical orientation and ~0.75 m in the horizontal orientation when the instrument is carried along the surface and assuming a homogeneous earth [*McNeill*, 1980]. Electromagnetic induction exploits contrasts in soil geophysical response, in this case the electrical response, to estimate soil textural [*Doolittle et al.*, 1994; *Robinson et al.*, 2008b; *Triantafilis and Lesch*, 2005] and hydrologic patterns [*Triantafilis et al.*, 2001]. Combining EMI surveys and soil water sampling has been used to estimate changes in soil water content when the differences in water content do not lead to measurable differences in other soil properties that also affect conductivity [*Sherlock and McDonnell*, 2003].

[5] Soil moisture dynamics are a critical system attribute in the integration of geophysical properties, hydrology, and ecosystem structure and function (Figure 1). Georeferenced EMI measurements provide noninvasive, rapid, and spatially continuous information about the changes in soil spatial properties and moisture at the landscape scale [*Abdu et al.*, 2008; *Hendrickx and Kachanoski*, 2002; *Sheets and Hendrickx*, 1995]. The purpose of the current study, building upon previous EMI measurement techniques [*Robinson et al.*, 2008a, 2009], is to investigate two cases of soil resource heterogeneities that affect the organization of

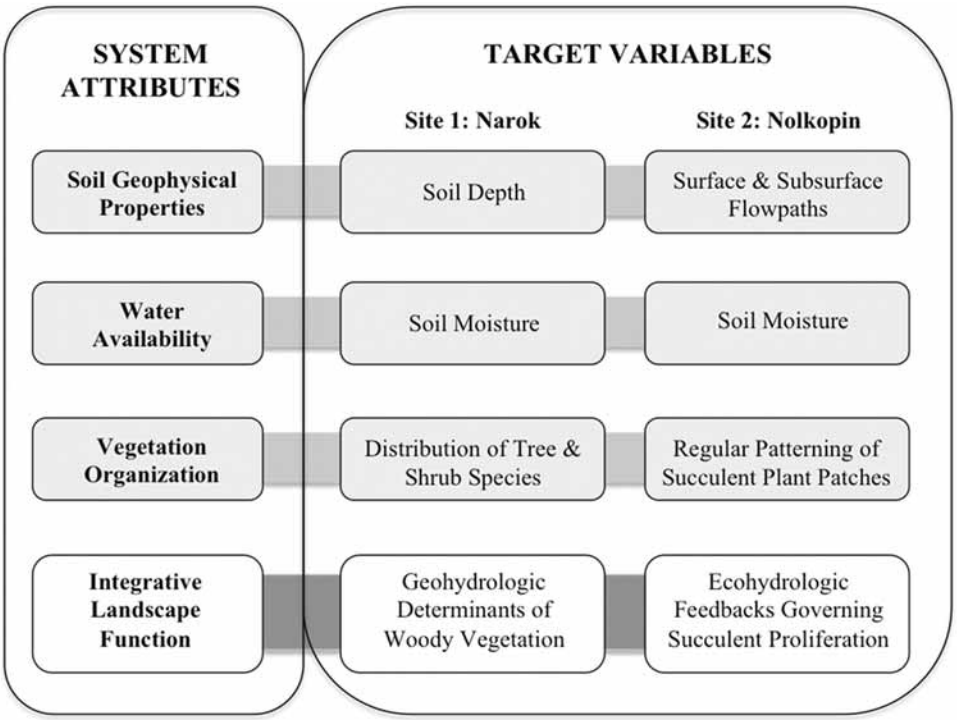

Figure 1. (left) The general geophysical, hydrological, and ecological system attributes (gray boxes) used to generate an integrated understanding of landscape function (white box). (right) For the Narok and Nolkopin study sites, we identified and measured specific target variables representing the system attributes (gray boxes), in order to understand key system processes governing landscape function (white boxes) at each site.

dryland vegetation patterns. The first case examines the relationship between soil depth and the spatial distribution of vegetation communities on hillslopes, and the second case investigates the spatial patterns of soil moisture inside and outside vegetation patches following rain events to identify feedbacks that may generate a regular pattern formation.

[6] The first case study is situated in a typical tree-grass savanna site in central Kenya (herein referred to as Narok), which exhibits characteristic topography and vegetation types of the region. The dominant vegetation at Narok is composed of two woody species, *Acacia tortilis* and *Acacia etbaica*, with a continuous herbaceous layer of perennial grasses and the succulent *Sansevieria robusta*. Previous studies have characterized *A. tortilis* as having both a shallow, wide-spreading root system and a deep tap root that uses hydraulic lift to utilize deeper water sources [*Dharani*, 2006; *Ludwig et al.*, 2003]. Comparatively, *A. etbaica* has been shown to be a very drought tolerant species in drylands [*Gebrehiwot et al.*, 2005]. *Sansevieria robusta* is one of three species in the genus that is common in open savannas in this landscape. It typically forms dense patches on the order of 2–10 m in diameter. At the Narok study site the *S. robusta* patches have remained relatively small and static over time, in contrast to the patches of a different *Sansevieria* species, *S. volkensii*, that occur in the second case study, discussed below. Our objective for the first case study was to use EMI surveys, vegetation mapping, and a simple geophysical model to construct a spatially continuous map of soil depths, in order to investigate the relationship between soil properties with the associated overlying vegetation communities (Figure 1).

[7] The second case study is situated in a more degraded savanna, herein referred to as Nolkopin, where intense grazing in recent decades has caused a transition in the herbaceous layer from subdense, fairly continuous perennial grass cover, to a matrix of large bare soil patches with sparse patches of mostly annual grasses. Concomitantly at this site, and in many similar degraded sites in the region, the native succulent *S. volkensii* has proliferated from an infrequent plant to form distinct, dense patches ranging in size from 2 m to 2 km wide [*King et al.*, 2010]. The expansion of barren areas appears to have altered the system hydrology, where runoff and run-on dynamics of surface water redistribution are now prevalent and readily visible. Our objectives at this site were to investigate both spatial and temporal heterogeneity in soil moisture to ascertain whether the patterns of surface flow and infiltration, and interactions with vegetation, may generate feedbacks that impel the continued expansion of *S. volkensii*. To do so, we employed EMI observations in and around *S. volkensii* patches where run on and runoff flow paths were obvious, then we used a numerical model to quantify the horizontal and vertical subsurface redistribution of water. From the numerical model, we aimed to assess the potential positive feedback mechanism that may facilitate the proliferation of *S. volkensii* (Figure 1). Understanding the impact of this mechanism to the *S. volkensii* and surrounding vegetation community is crucial for long-term management strategies to return the ecosystem to its native tree-grass state.

[8] The remainder of the paper is organized as follows. In section 2, we describe the study sites in central Kenya, the methods for field measurements and analyses, and modeling employed in association with each case study. Section 3 first presents calibrated electrical conductivity maps for the Narok site, the results of a simple geophysical model deriving soil depth, and associations between soil characteristics and vegetation patterns. Next we present the combined analysis of time-lapse electrical conductivity maps, continuous point measurements of soil moisture, and vegetation pattern at the Nolkopin site. Section 3 concludes with hydrological numerical model results for the Nolkopin case study, which are used to quantify the horizontal and vertical redistribution of water following localized infiltration events. In section 4, we describe the mechanisms and feedbacks influencing the spatial patterns of vegetation for each case of soil resource heterogeneity. We also identify limitations of the current study that should be addressed in future work.

2. Methods

2.1. Study Sites

[9] We investigated two cases of soil resource heterogeneity that affect the organization of the vegetation structure and patterns. At the Narok study site, we investigated the role of variations in soil depth as a control of soil resources with regard to biotic/vegetation spatial patterns; at the Nolkopin study site we conducted a small scale experiment imaging soil moisture wetting patterns around vegetation patches. Our two study sites were located 9 km apart in the Upper Ewaso Ng'iro river basin of the central Kenya highlands. The annual climate consists of two rainy seasons, March–May and October–December with nearly equal seasonal totals. The mean annual precipitation (MAP) is 450 mm yr^{-1}, the growing season average storm depth is 8 mm, and the growing season interstorm arrival rate is 0.19 d^{-1} [*Franz et al.*, 2010]. Forty soil texture samples collected over the top 40 cm around the Nolkopin study site were used to classify the soils as a sandy clay loam (sand, mean 55.49% [SD 5.99%], silt, 12.68% [2.06%], clay 31.82% [6.44%]), with a porosity of 0.45 (SD 0.0301) determined from 11 samples. The vegetation at the study sites is a typical savanna ecosystem composed of woody vegetation (mostly *Acacia tortilis, A. mellifera*, and *A. etbaica*) and grasses (commonly *Cynodon, Pennisetum, and Eragrostis* species) [*Dharani*, 2006; *Franz et al.*, 2010; *Young et al.*, 1995, 1998]. These rangelands support three primary land uses: traditional subsistence pastoralism, commercial cattle ranching, and nature conservancy, which are practiced at scales ranging from 1000 to 10,000 ha. All land use depends on primary productivity, vegetation structure, and composition; traditional pastoralists' livelihoods are particularly tightly coupled to vegetation for their basic sustenance [*Fratkin et al.*, 2004].

[10] The Narok study site (0°31′22″N, 36°51′45″E, elevation was 1580 m, mean slope was 5%) was located within a nature conservancy run by the Mpala Research Centre. It experiences light livestock grazing and abundant use by wildlife, and represents a typical tree-grass savanna system. We conducted measurements on a single hillslope covering an area of 6.25 ha of this complex terrain with isolated trees, clumps of trees, patches of the large-leaf succulent *S. robusta*, and some rock outcrops. The Nolkopin

study site (0°31′54″N, 36°56′18″E, elevation was 1700 m, mean slope was 3%) was located on communal Maasai lands, where extensive land degradation is associated with increased human and livestock populations and reduced mobility over the last five decades, as has occurred in other Kenyan drylands [*Fratkin*, 1997; *Fratkin and Mearns*, 2003; *Fratkin et al.*, 2004; *Mwangi*, 2007; *Njenga*, 2001]. At this site, the transition from a tree-grass to a bare tree mosaic has coincided with the proliferation of *S. volkensii* in intercanopy areas [*King et al.*, 2010]. *S. volkensii* is an undesirable species because it is unpalatable, and its spear-like leaves prevent livestock from foraging on other vegetation inside the patches. The widespread increases in bare areas have altered the hydrological functioning of the system, leading to an increase in Hortonian overland flow. Runoff plots (4 × 4 m) near the study site indicate approximately two to five times greater runoff in bare areas versus vegetated areas (Franz et al., An ecohydrological approach to predicting hillslope scale vegetation patterns in dryland ecosystems, submitted to *Water Resources Research*, 2011). Onsite observations indicated widespread rill and gully development, likely due to increased flow velocities and surface mounding at hummocked sites of permanent vegetation.

2.2. Narok Study: Field Methods

[11] We used electromagnetic induction (EMI) to estimate the spatial distribution of bulk soil electrical conductivity, EC_a (mS m^{-1}), following the methods used in previous studies [*Abdu et al.*, 2007; *Jones et al.*, 2005; *Robinson et al.*, 2008a, 2009]. We performed the EMI spatial mapping with the Dualem 1-S sensor (Dualem Inc., Milton, ON) combined with a Trimble Pro-XRS global position sensor (Seiler Instrument and Manufacturing Company, Inc., St. Louis, Mo.). Because we were primarily interested in the top 1.5 m of soil, we selected the Dualem-1-S sensor with 1 m coil spacing. In addition, the instrument was selected because of the low expected soil EC_a values [*Kiome and Stocking*, 1993], making instrument calibration easier compared to other available EMI sensors which require more onsite calibration tests [*Abdu et al.*, 2007].

[12] At the Narok site, we used a single day, reconnaissance style, high-spatial resolution EMI observational strategy following *Robinson et al.* [2008a] to understand the relationship between soil properties, particularly soil depth, and the spatial distribution of vegetation communities. On 24 March 2009, we surveyed (instrument carrying height was 30 cm) a 250 × 250 m area, walking in a serpentine pattern with a 3 m line spacing, recording a measurement every second for a total of ~18,000 data points. In the following days we used a GPS to map the canopy extent of all notable vegetation and land cover features (shrub patches, tree canopies, rock outcrops, and visible termite mounds) in the survey area.

2.3. Narok Site: Data Analysis

[13] The EC_a measurements were checked for quality and outliers were removed. By examining the GPS speed (the distance between data points collected every second), any redundant observations were removed from the data set when the mapper was stationary and the height of the instrument may have changed. No EC_a soil temperature correction was needed for Narok, because the survey was collected on the same day. Following these QA/QC procedures [*Robinson et al.*, 2009], a normal score transform procedure was used to transform the data [*Goovaerts*, 1997] into a Gaussian distribution with the SGEMS software package [*Remy*, 2005]. The normal score- transformed data were then fitted with a semivariogram and simple-kriged on a 1-m grid. After kriging, the data were back-transformed to produce a final kriged EC_a image. By using the individual fit of the semivariogram to account for spatial correlation, the kriging operation produced a smoothed data set that mitigated measurement uncertainty. The smoothed data set was then used in the inversion procedure without further consideration of measurement uncertainty. An alternative strategy for accounting for the uncertainty of geophysical measurements directly in the inversion procedure will be discussed in the next section.

[14] In order to estimate conductivity and depth of each soil layer, different geophysical models were used to invert the smoothed EMI EC_a data. In the current study we used simple layered geophysical models with the assumptions presented by *McNeill* [1980] with no lateral constraints. The lateral constraints of the measurements were accounted for in the geostatistical kriging analysis. An alternative strategy would be to include the lateral constraints directly in the inversion procedure, as extensively discussed in the work of *Auken et al.* [2005], *Christiansen et al.* [2007], *Siemon et al.* [2009], and *Viezzoli et al.* [2008]. As a whole, the hydrogeophysical community is still trying to understand coupled inversion methods for obtaining the highest quality data [*Ferré et al.*, 2009; *Hinnell et al.*, 2010]. In order to help resolve these coupled inversion procedures, we present here our assumptions and results of a simplified layered inversion procedure with the extensions to a more rigorous hydrogeophysical analysis.

[15] The Dualem sensor collects two simultaneous measurements depending on the transmitter and receiver coil orientations at each spatial location. The relative sensitivity of each measurement orientation is given by

$$h(d) = 1 - \frac{1}{(4d^2+1)^{\frac{1}{2}}}, \qquad p(d) = \frac{2d}{(4d^2+1)^{\frac{1}{2}}}, \tag{1}$$

where $h(d)$ is the horizontal–horizontal orientation depth sensitivity, $p(d)$ is the perpendicular–horizontal orientation depth sensitivity, and d (m) is the vertical downward distance from the sensor boom [*McNeill*, 1980]. The simplest geophysical model consists of one single conductive layer known as the homogeneous earth model given by

$$c_h = [1 - h(a)]e, \qquad c_p = [1 - p(a)]e, \tag{2}$$

where c_h (mS m^{-1}) is the integrated horizontal–horizontal EC_a measurement (HCP), c_p (mS m^{-1}) is the integrated perpendicular–horizontal EC_a measurement (PRP), a (m) is the instrument carrying height above the ground surface, and e (mS m^{-1}) is the conductivity of the homogeneous

earth. More complex models consist of multiple layers lying over the top of a uniform earth. The single layer model is given by

$$c_h = [h(a+t) - h(a)]s + [1 - h(a+t)]e,$$
$$c_p = [p(a+t) - p(a)]s + [1 - p(a+t)]e, \quad (3)$$

where t (m) is the depth of the conductive layer s (mS m^{-1}).

[16] In order to select an appropriate geophysical model for data inversion, we selected five random locations around the study sites to perform vertical soundings of the soil profile. At the different locations we collected data at 10 cm intervals from the ground surface to a height of 1.5 m above the ground surface. Using the various geophysical models we found the optimal parameters with a nongradient search algorithm by minimizing the sum of the residuals between the data and fit line. Previously excavated soil pits from around the study sites revealed that soils were between 1 and 2 m in three pits and greater than 2 m in one pit. The description of the study area from the 1980 UNESCO soil survey indicates that the soils are sandy clay loam with soil depths between 0.5–2 m with an underlying gneiss bedrock formation. As an added constraint to the inversion procedure, we set a low conductivity value (0.01 mS m^{-1}) for the resistive bedrock layer. The added constraints had minimal impact on the sum of residuals (see section 3.1) but allowed us to eliminate one unknown from the inversion procedure leaving two equations and two unknowns for a direct solution. The constrained single soil layer geophysical model, which simultaneously solves for the conductivity and depth of the soil layer using the HCP and PRP data, was found to be satisfactory for inverting the spatial EC_a values. Finally, we note that we set the maximum depth of soil at 2 m, which is the approximate penetration depth of the instrument under the homogeneous earth assumption [*McNeill*, 1980].

[17] To investigate associations between soil depth and vegetation and land cover patterns, we used the GPS data of canopy and surface cover features to pool the modeled soil depth information for each feature type, and then estimated the mean and variance of soil depth for each feature type. We compared the different sample means using the Kruskal-Wallis nonparametric test at the 95% significance level [*Walpole et al.*, 2002].

2.4. Nolkopin Site: Field Methods

[18] At Nolkopin, data logging sensors were used to determine the daily rainfall, soil temperature, and soil moisture for different patch types (bare soil, perennial grass, and two *S. volkensii* patches). Beginning in May of 2008, we installed a tipping bucket rain gauge (TE525, Campbell Scientific Inc., Logan, UT), time-domain reflectometry soil moisture sensors at 15 and 30 cm depth, oriented horizontally in each patch type (CS616, Campbell Scientific Inc., Logan, UT), and soil temperature probes at 15 cm depth, oriented horizontally in each patch type (108, Campbell Scientific Inc., Logan, UT); data were collected every 20 min. The probes were inserted in the upslope direction in order to minimize disturbance effects from the original excavation. We present the data as aggregated daily values and average the soil moisture measurements for a value representative of the top 40 cm. We corrected each soil moisture probe for temperature and calibrated the probes with volumetric water samples collected in April and July 2009 following the work of *Kelleners et al.* [2005].

[19] On 9 April 2009, we collected auger soil samples at 10 locations for depths of 20 and 40 cm, which were used to determine moisture and texture. Two samples were collected upslope of a *S. volkensii* patch, two samples below the patch, and six samples inside the patch. We determined volumetric water content (cm^3 cm^{-3}, samples dried for 24 hs at 105°C), and sent the soil samples to the Pedology Laboratory at the University of Idaho for soil texture, pH (log[H +]), and electrical conductivity of saturation paste extract, EC_w (mS m^{-1}). We repeated the soil sampling procedure on 27 July 2009, collecting samples at 30 locations in six rows and five columns in a uniform sampling grid around the same *S. volkensii* patch, with 16 samples outside the patch and 14 inside the patch.

[20] At Nolkopin we used a time-lapse EMI observational strategy following the work of *Robinson et al.* [2009] to understand the spatial patterns of soil moisture change following rain events. We repeatedly surveyed a 100 × 60 m area that included four distinct patches of *S. volkensii* (5–20 m in diameter) and the data logging sensors (with an instrument carrying height of 30 cm, 2 m line transect spacing, with ~3500 data points per sampling date). We surveyed before, and every 3 d following, two different rain events: a 15 mm rain event on 6 April 2009, and a 6 mm event on the 24–25 July 2009.

[21] In addition to the EMI surveys, we visually assessed evidence of surface water flow and erosion in order to delineate the vegetation patch margins into surface run on (surface water flow entering the *S. volkensii* patch) and runoff zones (surface flow out of or adjacent to the patch margins). At least two individuals independently delineated each patch margin, and in all cases, delineations agreed to <2 m. Patch margins themselves were also delineated and mapped with the GPS.

2.5. Nolkopin Site: Data Analysis

[22] We applied the same quality control, normalizing, kriging, and single-layer inversion methods to the Nolkopin site EC_a data as were used at the Narok site, with one exception: to account for variation in soil temperature among repeated surveys of the Nolkopin site, we used the time series of soil temperatures from CS616 probes to correct each set of survey EC_a values to a temperature of 25°C [*Sheets and Hendrickx*, 1995]. Following rain events, cooler rainwater may result in temperature changes of 5°C–7°C in the soil, resulting in changes of conductivity of up to 10%–15% following the work of *Sheets and Hendrickx* [1995].

[23] We used multiple regression to analyze correlations between physical properties of augered soil samples and EC_a values recorded the day of the soil sampling. We also visually evaluated the spatial images of EC_a in the study area in order to relate gross differences in the background EC_a signal to additional observed abiotic and biotic conditions. Next, we analyzed the effects of run on versus runoff zones and the effects of distance from patch margin on the prepost rainfall changes in EC_a. For each kriged pixel within 4 m (inside or outside) of a patch margin, we calculated the difference between the initial (dry) EC_a value and EC_a at 3, 6, and 12 d after each rain event. Each pixel was classified as adjacent to

either a run on or a runoff zone. Pixels were also classified according to their distance inside or outside the patch margin in 1 m increments radially outward. We then pooled pixels by zone type and distance category, and estimated the mean and standard error change in EC_a at each time step.

2.6. Numerical Modeling

[24] In order to help interpret the observations of the EMI imagery for Nolkopin, we used a quasi 3-dimensional numerical solution of Richard's equation [*Pinder and Celia*, 2006, equation (4.36)] to simulate the redistribution of water in the top 40 cm of the subsurface following rain events. The domain consisted of two vertically averaged soil layers with an underlying impermeable bedrock layer, which defined the lower boundary condition. Because we were motivated by differences in the initial conditions due to localized vertical infiltration in run on and runoff zones, we used a homogeneous isotropic soil for both layers; see Table 1. We used a 90 × 70 m domain with 2 × 2 m grid cells, where the topsoil layer was 0.4 m thick and the bottom soil layer was 0.6 thick, both at a slope of 3%. The parameters were consistent with field observations at Nolkopin, where excavation pits indicated *S. volkensii* rooting depths of 30–40 cm and a bedrock layer at a depth of 1–2 m. We chose the domain size to include the relative locations of the two largest *S. volkensii* patches in a surrounding bare soil matrix.

[25] The rectangular domain consisted of four no-flow boundary conditions that did not influence the solution. The top boundary condition (sink term Q in the vertically averaged equation (4.36) by *Pinder and Celia* [2006]) represented the evapotranspiration losses to the atmosphere. We assumed soil moisture loss (evapotranspiration) during interstorm periods followed an exponential decay, which allowed us to use a decay constant, k ($m^3\ m^{-3}\ d^{-1}$) defined for each patch type. We used CS616 daily soil moisture to estimate the average decay constant for each patch type (bare soil was 0.0664 $m^3\ m^{-3}\ d^{-1}$, *S. volkensii* was 0.04 $m^3\ m^{-3}\ d^{-1}$). The total daily water use or evapotranspiration (mm d^{-1}) for each unit area is the product of the decay constant, layer thickness (assumed to be 40 cm for *S. volkensii* rooting zone), and water content resulting in maximum daily evapotranspiration rates (at well-watered conditions, see Table 1) for bare soil at 7.0 mm d^{-1} and *S. volkensii* at 4.2 mm d^{-1}, which is consistent with estimates in this dryland ecosystem [*Franz et al.*, 2010]. The lower boundary condition for the topsoil layer (the sink term Q in the vertically averaged equation (4.36) by *Pinder and Celia* [2006]) represented leakage or vertical redistribution between the two soil layers. We represented the flow between the two soil layers by the 1-dimensional vertical form of Darcy's law [*Pinder and Celia*, 2006, equation (4.35)]. The vertical distance between the top and bottom soil layer's centroids was assumed to be 0.5 m. The lower soil layer saturation (ratio of volumetric water content to porosity) was held constant at 0.30, based on volumetric water content samples collected during the dry season (Table 2). Estimates of drying depths following stage-1 evaporation (liquid stage) for sandy clay loam are between 21 and 56 cm [*Lehmann et al.*, 2008; *Shokri et al.*, 2009]. Given the high evaporative demand (bare soil was 7.0 mm d^{-1}) and length of dry season (3–4 months), drying fronts may be well into stage-2 evaporation (the gaseous stage) [*Lehmann et al.*, 2008], with low soil moisture values approaching 1 m in depth by the beginning of the wet season. In addition, observations from nearby CS616 sensors at 70 and 100 cm indicated less than 10% of rain events impacted probes at these depths (Franz et al., submitted manuscript, 2011), justifying the assumption of a constant saturation for small- and medium-sized rain events for this lower soil layer.

Table 1. Summary of Soil Characteristics at Nolkopin (0°31′54″N, 36°56′18″E)

Soil Characteristics	Values
Porosity, ϕ[a]	0.45
Residual volumetric water content, θ_r[b] ($cm^3\ cm^{-3}$)	0.080
Field capacity volumetric water content, θ_{fc}[c] ($cm^3\ cm^{-3}$)	0.264
van Genuchten shape parameter, n[b]	1.3484
van Genuchten shape parameter, α[b] (cm^{-1})	0.0209
Pore-connectivity parameter, l[b]	0.5
Saturated hydraulic conductivity, K_s[b] (cm d^{-1})	27.74

[a]Value estimated as mean of onsite sampling (sample number = 11, SD = 0.0301).

[b]Values estimated from HYDRUS and Rosetta-lite program with mean sand = 55%, silt = 13%, clay = 32%, and bulk density = 1.382 derived from onsite sampling [*Schaap et al.*, 2001; *Simunek et al.*, 2006].

[c]Value estimated from van Genuchten pressuresaturation relationship with assumption that $\psi_{fc} = -0.033$ MPa [*Rodriguez-Iturbe and Porporato*, 2004].

[26] We used the soil texture laboratory results to estimate the van Genuchten model parameters, which define the pressure-saturation water release curve for the soil (Table 1) [*Schaap et al.*, 2001; *Simunek et al.*, 2006; *Vangenuchten*, 1980]. A simple power function was used to represent the unsaturated hydraulic conductivity function [*Pinder and Celia*, 2006, equation (11.17)]. On the basis of a sensitivity analysis using the CS616 and EMI images, we found a value of five for the exponent to give satisfactory fit for the unsaturated flow behavior. We note that a more rigorous analysis estimating unsaturated flow parameters using an inverse solution procedure may be performed if sufficient data are available [*Franz et al.*, 2011; *Simunek et al.*, 2006].

[27] The initial conditions in the topsoil layer were selected on the basis of general observations from the EMI survey following the 6 April 2009 rain event. In patch run on zones and the first level of neighbors, we used initial saturations between 0.50 and 0.70 selected randomly from a normal distribution (with a scaled mean of 0.6 and variance of 1). In patch runoff zones and the first level of neighbors, we used initial saturations between 0.25 and 0.50 selected randomly from a normal distribution. The remainder of the topsoil layer in the domain was set to an initial saturation of 0.25, which is near residual saturation. The system was solved with a time-adaptive finite difference scheme using upstream weighting [*Pinder and Celia*, 2006].

3. Results

3.1. Comparison of Ec_a With Landform and Vegetation Spatial Patterns

[28] The results of the geophysical model data inversion for five random vertical sounding locations are provided in Figure 2 and Table 3. The results of the model fitting indicate that the single-layer soil model with underlying bedrock provides a satisfactory fit as would be expected for this soil that shows little horizonation, as the sum of residuals does

Table 2. Summary of Volumetric Water Content Samples Collected Over Time

	Sample Depth (cm)		
	10–30	30–50	50–70
July 2006, Near Nolkopin, No Rainfall in 18 Months			
Mean volumetric water content (cm^3 cm^{-3})	0.075	0.093	0.116
SD	0.0298	0.0475	0.0350
Sample number	7	5	4
April 2009, Nolkopin, 3 Days After 15 mm Rain Event			
Mean volumetric water content (cm^3 cm^{-3})	0.117	0.121	-
SD	0.0410	0.0209	-
Sample number	10	10	-
July 2009, Nolkopin, 3 Days After 6 mm Rain Event			
Mean volumetric water content (cm^3 cm^{-3})	0.093	0.102	-
SD	0.0451	0.0195	-
Sample number	30	30	-

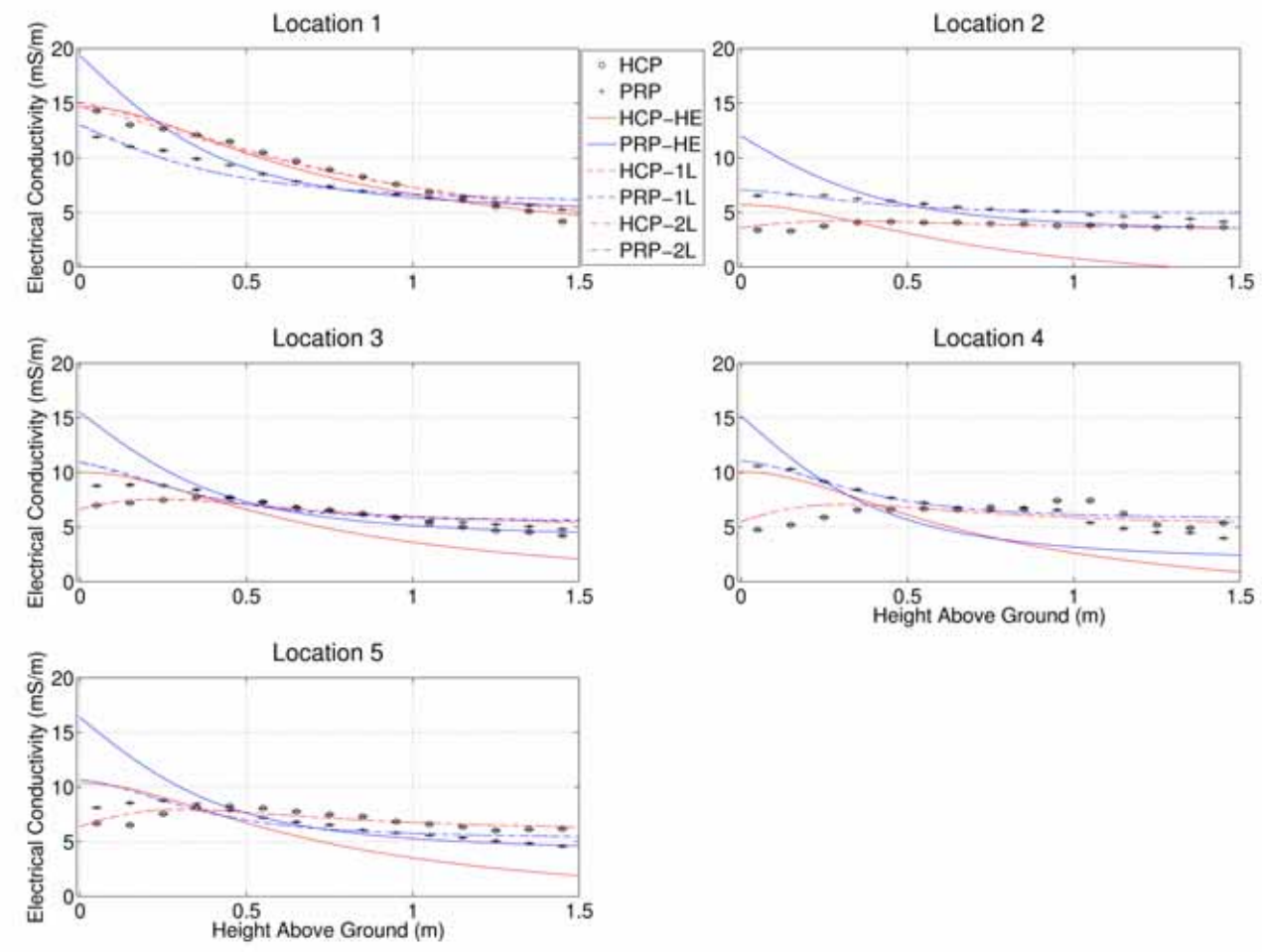

Figure 2. Geophysical model fits of EMI vertical sounding data at five random locations with resistive bedrock constraint. HCP and PRP are measured electrical conductivity in the respective EMI coil orientations, HE is the homogeneous earth model, 1L refers to the single soil-layer model with underlying homogeneous earth, and 2L refers to the two soil-layer model with underlying homogeneous earth.

Table 3. Summary of Parameter Fitting for Different Geophysical Models at Five Randomly Selected Vertical Sounding Locations

		Vertical Sounding Location				
		1	2	3	4	5
Geophysical EMI Model	Number of Fitting Parameters	Sum of Residuals				
Homogeneous Earth	1	20.95	42.16	36.33	65.47	49.30
1 Layer	3	8.86	5.26	9.62	14.70	11.46
2 Layer	5	8.86	5.26	9.56	14.70	11.46
3 Layer	7	7.68	5.26	9.33	14.70	11.46
		With Resistive Bedrock Constraint				
Homogeneous Earth	-	-	-	-	-	-
1 Layer	2	13.81	5.28	10.49	14.71	15.29
2 Layer	4	9.28	5.27	10.49	14.71	11.47
3 Layer	6	9.00	5.27	10.49	14.71	11.47

not significantly decrease with additional model complexity. In addition, the sum of residuals is moderately affected in two of the five locations, indicating that the resistive bedrock layer constraint does not greatly affect the model fits (Table 3, row 3 versus row 8 for the single-layer soil model). Instead of performing labor intensive and time consuming vertical soundings at each spatial location in the area, the single-layer soil model (equation (3)) solved for the two unknowns (soil depth and conductivity) simultaneously and uniquely using only the HCP and PRP for each spatial location at one carrying height. For the current analysis we assumed the inversion procedure was independent between spatial locations and instead included the spatial correlation in the geostatistical analysis of the EC_a data (section 2.3). While this assumption greatly reduced time and labor in the field, a more formal hydrogeophysical inversion may be required to accurately account for the inherent uncertainty [*Auken et al.*, 2005; *Christiansen et al.*, 2007; *Siemon et al.*, 2009; *Viezzoli et al.*, 2008].

[29] Table 4 summarizes the patch characteristics in the study plot with the mean and standard deviation of modeled soil depth. Table 4 also summarizes the results from 28 randomly located hand-augered sites around the site. Because we were unable to auger to the bedrock by hand at all locations (auger length was only 100 cm), we grouped the samples into two categories, auger depth <25 cm and >50 cm. The modeled soil depth for the shallow auger samples (mean depth of 0.55 m) and deeper auger samples (mean depth of 1.51 m) were statistically different (Kruskal-Wallis $p < 0.05$). The data provide further validation in the single soil layer inversion analysis but with the caveat of low spatial coverage and a limited number of samples around the site.

[30] Figure 3 provides the modeled soil depth map with the associated canopy and landform features for the Narok hillslope. The southern boundary, running approximately west to east, is the top of the hillslope, and the difference in elevation is $\sim$20 m between the top and bottom of the surveyed area. The dominant feature illustrated by Figure 3 is the swath of deep soils running diagonally through the image. The shape, direction, and width of the deeper soil areas were not evident from surface conditions, except for the identified rock outcrops in shallower areas. *Acacia tortilis* trees were located on significantly deeper soils (mean depth of 1.41 m) than *A. etbaica* trees (mean depth of 0.54 m, Kruskal-Wallis $p < 0.05$).

3.2. Comparison of Time-Lapse Ec_a Soil Moisture in Different Vegetation Patches

[31] The time series of soil moisture, soil temperature, and rainfall from May 2008 to August 2009 at Nolkopin are summarized in Figure 4. The sets of probes in the two *S. volkensii* patches behaved very similarly throughout the time series: the grass patch CS616 was the most responsive to rainfall events, and its soil was the coolest. The bare soil CS616 was the least responsive to rain events and its soil was the warmest. During the relatively large 30–40 mm rain events in November 2008, (compared to average storm size of 8 mm in the region [*Franz et al.*, 2010]), the *S. volkensii* and grass CS616 probes followed a similar behavior of rapid jumps in soil moisture and exponential decays during interstorm periods. However, during medium (a 15 mm event in April 2009) and small events (a 6 mm in July 2009), the *S. volkensii* probes showed increased time-to-peak soil moisture responses of 3–5 d compared to 1–2 d and inverted parabolic interstorm decay shapes. The bare soil CS616 probe illustrates delayed time-to-peak responses and inverted parabolic interstorm decay shapes throughout the time series. The delayed time-to-peak response and

Table 4. Summary of Modeled Soil Characteristics, Associated Land Cover Patches, and in Situ Sampling at Narok (0°31′22″N, 36°51′45″E)

	Mean Soil Depth (m)	SD Soil Depth (m)	Total Surface Area (m^2)	Number of Patches/Samples
A. tortilis	1.41	0.103	1393	37
A. etbaica	0.54	0.179	210	11
Rock outcrop	0.29	0.247	71	5
S. robusta	1.61	0.093	6360	35
Termite mound	1.25	0.094	989	50
Auger depth <0.25 m	0.55	0.248	<1	5
Auger depth >0.5 m	1.51	0.666	<1	23

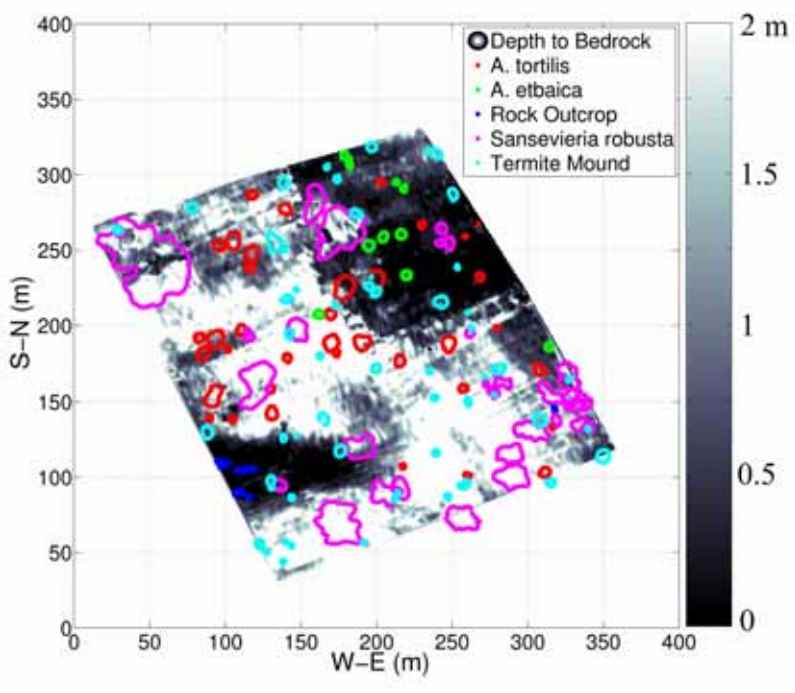

Figure 3. The model estimates of soil depth and spatial locations of vegetation/land formations at the Narok study site (0°31′22″N, 36°51′45″E). Colored outlines illustrate either the canopy or the spatial extent of vegetation/land formation.

inverted parabolic interstorm decay shapes indicate additional sources of water in the subsurface. By mass balance, the water sources are believed to be from nonlocal sources rather than strictly vertical infiltration from event water above the probes. This signature of nonlocal sources identified at the CS616 probes generated part of the motivation for the numerical modeling component of this study and subsequent analyses of EMI images.

[32] In order to interpret the EMI survey results, we first sought to better understand what soil parameters contribute the most to EC_a values. We investigated linear correlations of EC_a (HCP) to volumetric water content, clay percentage, soil pH, and saturation paste extract electrical conductivity averaged over the top 40 cm (Figure 5). We also included in the analysis the daily CS616 values corresponding to the EMI sampling days and locations. The linear regression indicated that EC_a was most strongly correlated to volumetric water content ($R^2 = 0.339$, $p < 0.001$), followed by clay percentage ($R^2 = 0.314$, $p < 0.001$), and soil pH ($R^2 = 0.125$, $p = 0.027$), and not correlated with the saturation extract conductivity ($R^2 = 0.0013$, $p = 0.829$). A multivariate linear regression using volumetric water content, clay percentage, and soil pH explained 53% of the variance in EC_a ($R^2 = 0.53$, $p < 0.001$). The remaining variation is likely due to variations in soil depth, soil nutrients, biotic effects, and sampling errors due to differences in auger sample size and CS616 support volume compared to the EMI averaging volume. The analysis demonstrated the direct relationship between EC_a measurements and measured changes in water content.

[33] The temperature corrected and smoothed EC_a images (HCP) of representative patches for the two rain events at Nolkopin are presented in Figure 6. The HCP data is presented, as it is more sensitive to changes in the top 40 cm than the PRP data (see equation (1)). The relative locations of the CS616 probes and *S. volkensii* patch boundaries are indicated in Figure 6f. Interpretation of the EC_a maps suggests two sets of findings, the first regarding a variation in the background EC_a signal at the site, and the second regarding vegetation effects on EC_a changes following rainfall.

[34] The prerain event (dry) EMI surveys (Figures 6a and 6f) indicated the background EC_a signal across the survey area. We used additional observations from the field site to evaluate gross variation in the background EC_a signal, which remained largely unexplained by the correlated soil physical properties. The low EC_a values in the upper left-hand side of the image appear to be associated with shallower soil, as we found that augering was not possible beyond 40 cm in this area due to the presence of large gravel. The positive EC_a elliptical area in the upper right-hand corner coincided with evidence of a large subterranean termite nest, indicated by numerous small, domed mounds constructed on the surface in that area following rains. While we could not determine the extent of the nest without fully excavating the site, excavated nests in Kenya have revealed soil modifications to spatial extents on the order of tens of meters [*Darlington*, 1997, 2005]. Termite nests located on sandy soils in drylands are typically higher in clay content [*Turner*, 2006], which would increase the EC_a value. In addition, termites store woody and leafy debris to cultivate their larvae, which may increase the EC_a value depending on the decompositional state of the debris [*Lee et al.*, 2004]. Finally, auger samples at this site were able to reach 70 cm indicating deeper soils, which will also contribute to the higher EC_a values. Additional vertical soundings and soil excavations coupled with an inversion analysis would help fully resolve these observed differences in the dry EMI survey.

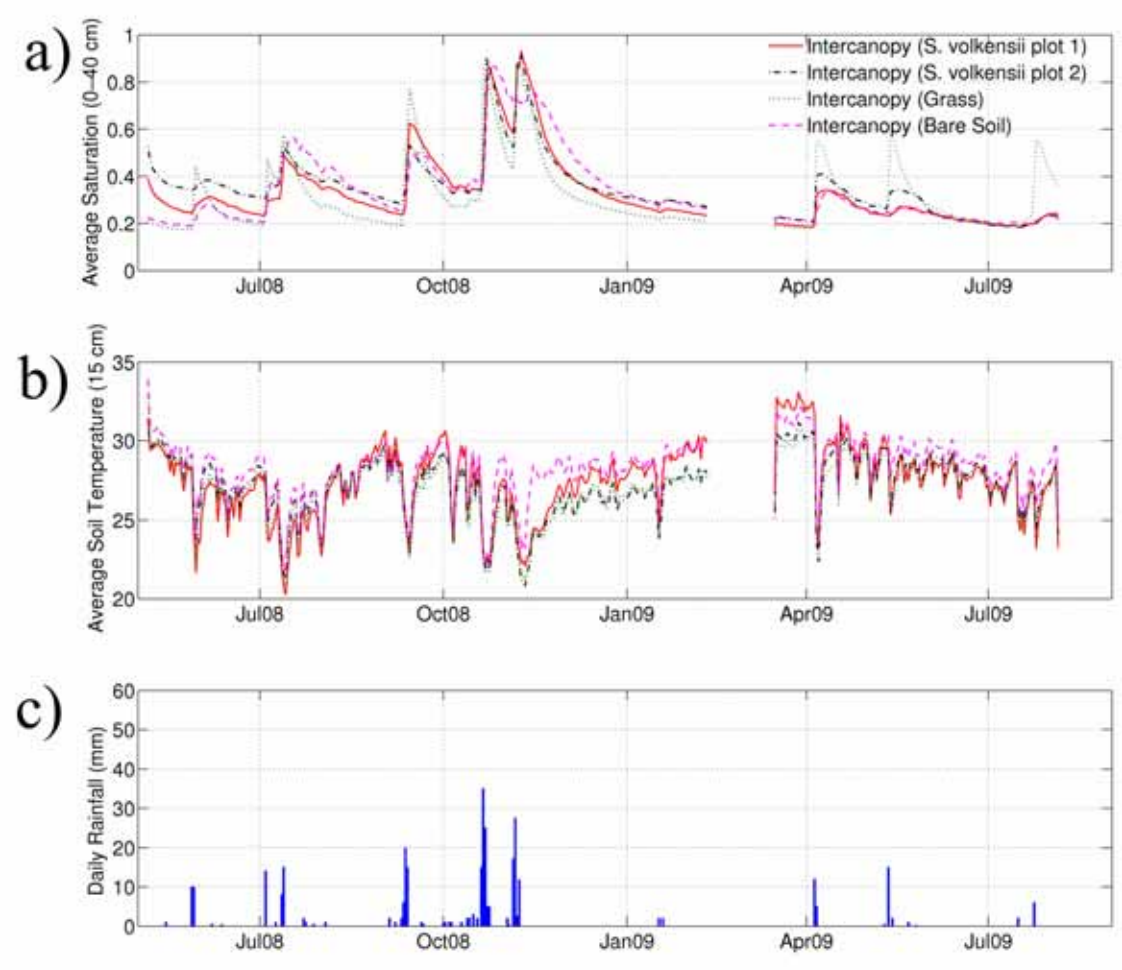

Figure 4. Time series of (a) average daily saturation in top 40 cm, (b) average daily soil temperature at 15 cm, and (c) daily rainfall at Nolkopin study site (0°31′54″N, 36°56′18″E).

[35] Figures 6a–6j show the increases and decreases in EC_a values after rain events. EC_a changes closely reflect changes in volumetric water content, since the other variables that affect EC_a (clay percentage, soil pH, and depth to bedrock) change on longer timescales. The patterns indicate that, in general, the rainfall events resulted in more noticeable changes in EC_a, and hence soil moisture inside the *S. volkensii* patches than in the interpatch areas. This pattern was hypothesized to be due to low infiltration in interpatches, coupled with run on capture and increased infiltration in *S. volkensii* patches. The examination of changes in EC_a along patch margins was conducted to seek further corroborative evidence for that mechanism.

[36] The general event response behavior along margins of the center *S. volkensii* patch is summarized in Figure 7. Figure 7 shows the change of EC_a with time for patch margins characterized as run on and runoff zones, and for different distances inside (negative values) and outside (positive values) the patch margin. The response of the patch to the 24–25 July 2009, 6 mm event indicated minimal differences inside and outside the patch (<1 mS m^{-1}) with slightly higher changes in EC_a in run on versus runoff zones (<0.5 mS m^{-1}). The patch response to the 6 April 2009, 15 mm event, however, showed much higher changes in EC_a in run on versus runoff zones (3 mS m^{-1}) and inside versus outside the patch boundary (1.5 mS m^{-1}). Finally, the initial variability in EC_a following rain (shown by the relative size of error bars on day 3) was much larger for the 15 mm event compared to the 6 mm event. The variability decreased with time as the water was redistributed in the subsurface and the soils dried out. The different responses of the patch to the two storm sizes suggests threshold behavior and will be discussed later.

[37] The changes in EC_a following the 15 mm event on 6 April 2009 presented in Figure 7b can also be visualized in the EC_a maps in Figures 6a–6e. The EC_a map in Figure 6b indicates the initial vertical infiltration, which is visibly concentrated along the top run on zones of the central patch, where surface run on would have been greatest. Figure 7b shows that on average, the initial increase in EC_a was 3 mS m^{-1} higher in run on zones compared to runoff zones. This equates to $\sim$0.10 cm^3 cm^{-3} of water, using the linear fit from the regression of EC_a and water content. However, since the image was collected 3 d after the rainfall, some redistribution of water had already occurred in the subsurface, and will be discussed in the next section. Continuing in time (Figures 6c and 6d), the saturated areas expanded to include more of the central patch and surrounding bare soil

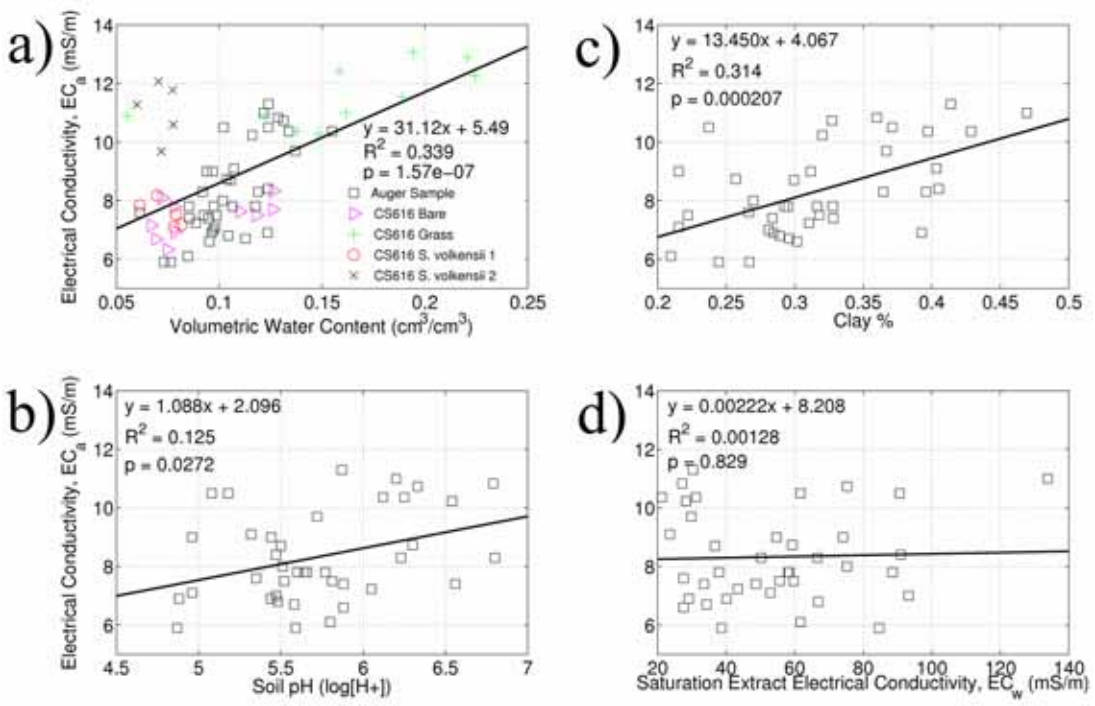

Figure 5. Correlation between bulk electrical conductivity and 40 soil auger samples of (a) volumetric water content, (b) soil pH, (c) clay percentage, and (d) saturation extract electrical conductivity averaged over top 40 cm at the Nolkopin study site (0°31′54″N, 36°56′18″E). Also included in the figue is the CS616 soil moisture data from each probe (averaged over top 40 cm) recorded on the 10 EMI sample dates.

areas outside the patch. This redistribution phenomenon is shown by Figure 7b in the run on +5 d line, where the points farthest from the patch edge have increased in value compared to the +3 d line. Figure 6e presents the drying out of the patches, with the image returning near to the dry initial conditions of Figure 6a.

[38] The subsurface water redistribution response seen in the EC_a imagery (Figures 6c and 6d) is also reflected in the CS616 probe time series. Looking at the CS616 responses for the April event (Figure 4), we see the grass probe initially wetted up to 0.55 saturation and decayed exponentially through time. However, the three remaining probes showed delayed time-to-peak responses of 3–5 d with increases in saturations to around 0.30 after that time period. In addition, the interstorm decays are shaped like inverted parabolas indicating a horizontal redistribution of water. The bare soil patch CS616 shows the most pronounced interstorm inverted parabolic shape, which corresponds to the subsurface redistribution seen in Figures 6c, 6d, and 7b. The smaller *S. volkensii* patch in Figures 6a–6e, however, did not respond in the same way. This may be due to its smaller contributing area dampening the run on effects and shallower soil depths dampening the EMI signal response in the soil.

[39] The EMI patch responses to a 6 mm event on 24–25 July 2009 are presented in Figures 6f–6j. The smaller rain event results in smaller vertical infiltration (changes in ECa <1 mS m^{-1}) with only a few localized pockets around the center patch and a run on zone of the far right patch as shown by Figure 7a. The rain event did not lead to significant redistribution of subsurface water as compared to the April storm. The lack of lateral redistribution of water is confirmed by the nonresponse of the *S. volkensii* and bare patch CS616 probes remaining near saturations of 0.20 (Figure 4). Vertical infiltration was still observed at the grass CS616 probe with a saturation increase to 0.55. The probe was located in a surface run on zone and had higher vertical infiltration than the compacted bare soil patch that was also located in this run on zone.

3.3. Numerical Model Results

[40] The results of the quasi 3-dimensional numerical model (vertically averaged soil layers) are summarized in Figure 8a. Figure 8b presents the mean and standard deviation of the redistribution process organized by run on and runoff zones and by distance from the patch margin (negative values into the patch). The objective of the idealized numerical simulations was to illustrate the horizontal redistribution of water from an initially perturbed saturation field. As a result of the large potential gradients, the reorganization of subsurface water from the initially perturbed saturation field is rapid with minimal effects occurring after day 6. The reorganization of water is evident in time by the shrinking error bars in Figure 8b; after day 6 only evapotranspiration is taking place. The mass balance of the 12 d simulation indicates that 96.6% of the water is lost to evapotranspiration and only 3.4% to vertical leakage into the lower soil zone, resulting in minimal changes in the average water content of this layer. By the end of the 12-d simulation, saturation conditions have nearly returned to the dry steady state condition at the residual saturation of 0.18.

[41] Nearly all of the horizontal and vertical redistribution of water takes place in the run on zones where saturations

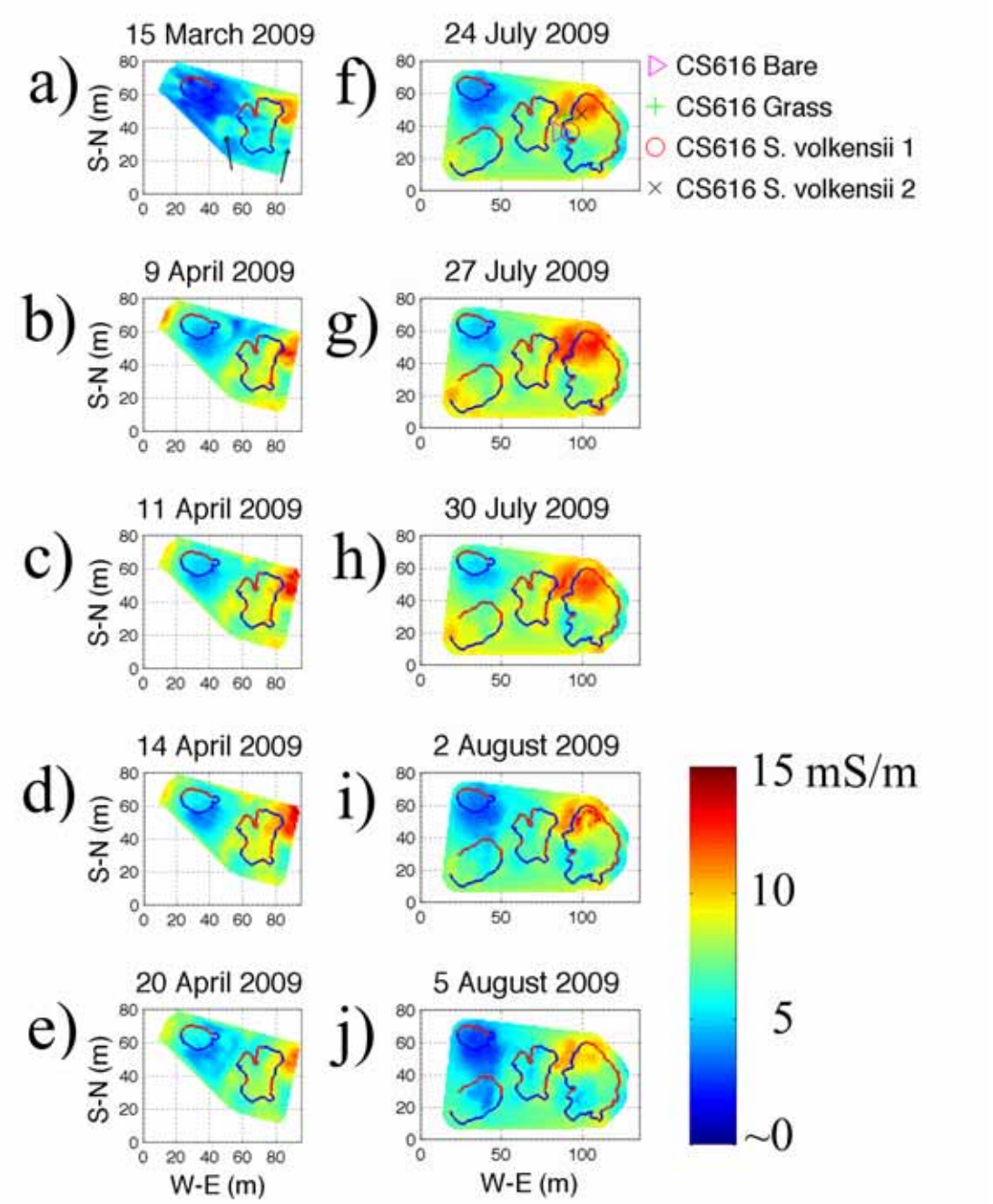

Figure 6. Bulk electrical conductivity maps and *S. volkensii* patch boundaries collected on different sampling dates at the Nolkopin study site (0°31′54″N, 36°56′18″E). Black arrows indicate the surface flow directions, colored symbols indicate the spatial locations of the CS616 probes, blue boundaries are surface run on zones, and red boundaries are surface runoff zones. Figures 6a–6e illustrate EMI surveys for dry conditions and surveys following a 15 mm rain event on 6 April 2009. Figures 6f–6j illustrate EMI surveys for dry conditions and surveys following a 6 mm rain event on 24–25 July 2009.

are above 0.50. Despite larger potential gradients at lower saturations, the hydraulic conductivity rapidly approaches zero at low saturations. In the run on zones, the water spreads vertically and horizontally with time, and patch margins in close enough proximity coalesce to form wider swaths of elevated saturation values. The daily run on lines in Figure 8b illustrate the spread of the water outward from the patch margins (5 and −5 m), where initial saturations of 0.25 increase to 0.35. In addition, the variance in this spreading is large with standard deviations outside the patch of 0.06 and 0.04 inside the patch. Comparatively, the runoff patch margins increase in saturation from 0.25 to 0.27 with standard deviations of 0.02. The differences in initial conditions between the run on and runoff zones leads to a "halo" of increased saturations around the run on patch margins in the topsoil layer. The impact of this "halo" of saturation may create a

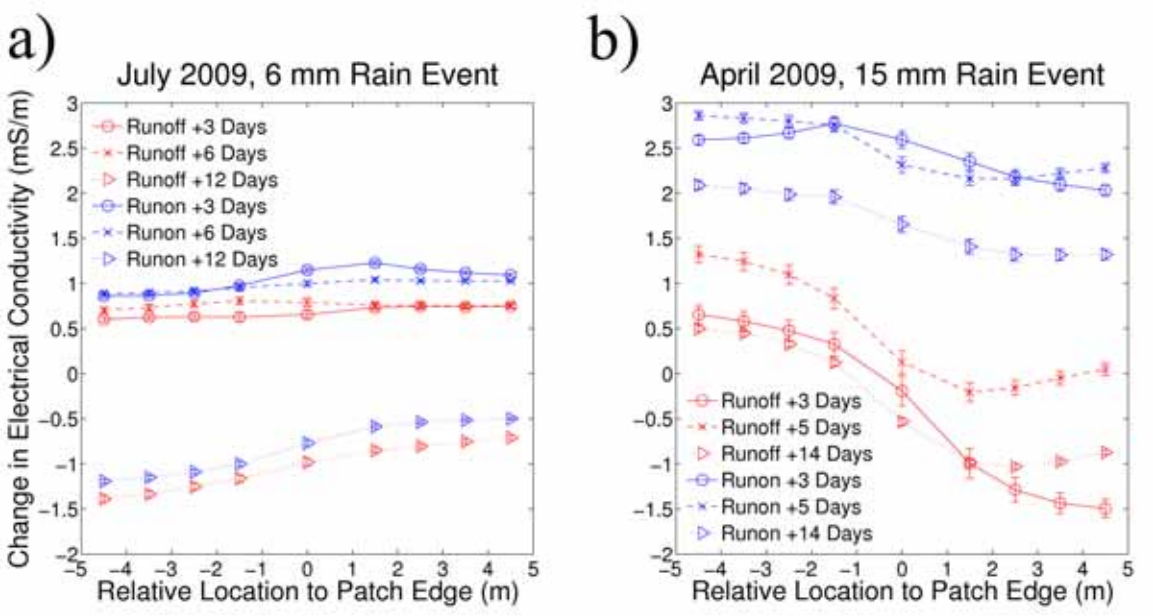

Figure 7. A summary of the differences in bulk electrical conductivity (±1 SEM) organized by time since the rainfall, run on versus runoff zone, and location to patch perimeter (radial transects with negative values inside patch) for two different sized rain events: (a) 6 mm on 24–25 July 2009 and (b) 15 mm on 6 April 2009 at the Nolkopin study site (0°31′54″N, 36°56′18″E).

local positive feedback mechanism impelling the expansion of *S. volkensii*, given its reproduction via below ground rhizomes, and will be discussed in the next section.

[42] In order to investigate the scale of the "halo" effect around *S. volkensii* patch margins, we conducted a simple numerical experiment exploring the redistribution of water due to different initial conditions and infiltration event sizes. A 2-dimensional Richard's equation (vertically oriented as opposed to the horizontal orientation described in section 2.6) was used to quantify the horizontal and vertical flux of water out of an initially saturated 0.5 × 0.5 m area in a 2 × 2 m domain (0.0625 m square grid cells) with no-flow boundary conditions (Figure 9a). Here the 0.5 × 0.5 m saturated area represented the preferential vertical infiltration around vegetation margins. The saturation depth profile was set to hydrostatic conditions (steady state), with varying saturations set at the lower 2 m boundary.

[43] Figure 9b presents the horizontal to vertical flux ratio over the parameter space, indicating that the ratio approaches 1 with decreasing initial saturation profiles. Physically, the effect of gravity becomes negligible as the potential gradients became large at lower saturation values, indicating that the flux is almost equally split between the horizontal and vertical directions. In addition, the length scale of the increased saturation is dependent on the initial conditions (Figure 9c). The horizontal effects are negligible for starting saturations of 1 and 0.6. However, the effects of the localized infiltration at a saturation of 0.25 are evident 3–4 times the length of the initially saturated area with redistribution occurring over several days. Volumetric water content measurements in the dry season indicated that conditions are near residual saturations for depths of 50 to 70 cm (Table 2). Estimates of drying fronts for sandy clay loam [*Lehmann et al.*, 2008; *Shokri et al.*, 2009] indicate depths of 21 to 56 cm by the end of stage 1 evaporation. Given the high variability of rainfall in this system (coefficient of variation for annual rainfall was 0.45 [*Franz et al.*, 2010]), entire rainy seasons frequently produce very little or no rainfall. For example, Nolkopin did not receive substantial rainfall for an 18-month period between 2005 and July 2006. After this period of time, the effects of stage 2 evaporation [*Lehmann et al.*, 2008] may produce dry soil moisture values in excess of 1 m, leading to initial conditions that would favor a significant amount of horizontal redistribution of subsurface water following localized vertical infiltration events.

4. Discussion

4.1. Evidence of Woody Vegetation Organization

[44] Geophysical imaging and data analysis from the Narok savanna study site revealed large subsurface features that were nearly undetectable from surface conditions. Using a simple geophysical model (equations (1)–(3) and Table 4), we constructed a spatial map of soil depths (Figure 3). The correlations between modeled soil depth, rock outcrop locations, and hand-auger sites provided corroboration that the simple model yielded reasonable results (Table 4). Noticeably, the two woody species had statistically significantly different mean soil depths, where *A. tortilis* preferred areas with deeper soil. Physiologically, *A. tortilis* has a deep tap root system and can use hydraulic lift to increase access to deeper water sources [*Dharani*, 2006; *Ludwig et al.*, 2003]. Comparatively, *A. etbaica* has been shown to be a drought tolerant species [*Gebrehiwot et al.*, 2005], which would have an advantage over *A. tortilis* on shallower soils where the number of soil moisture excursions and the length of excursions below the wilting point would lead to relatively higher stress values

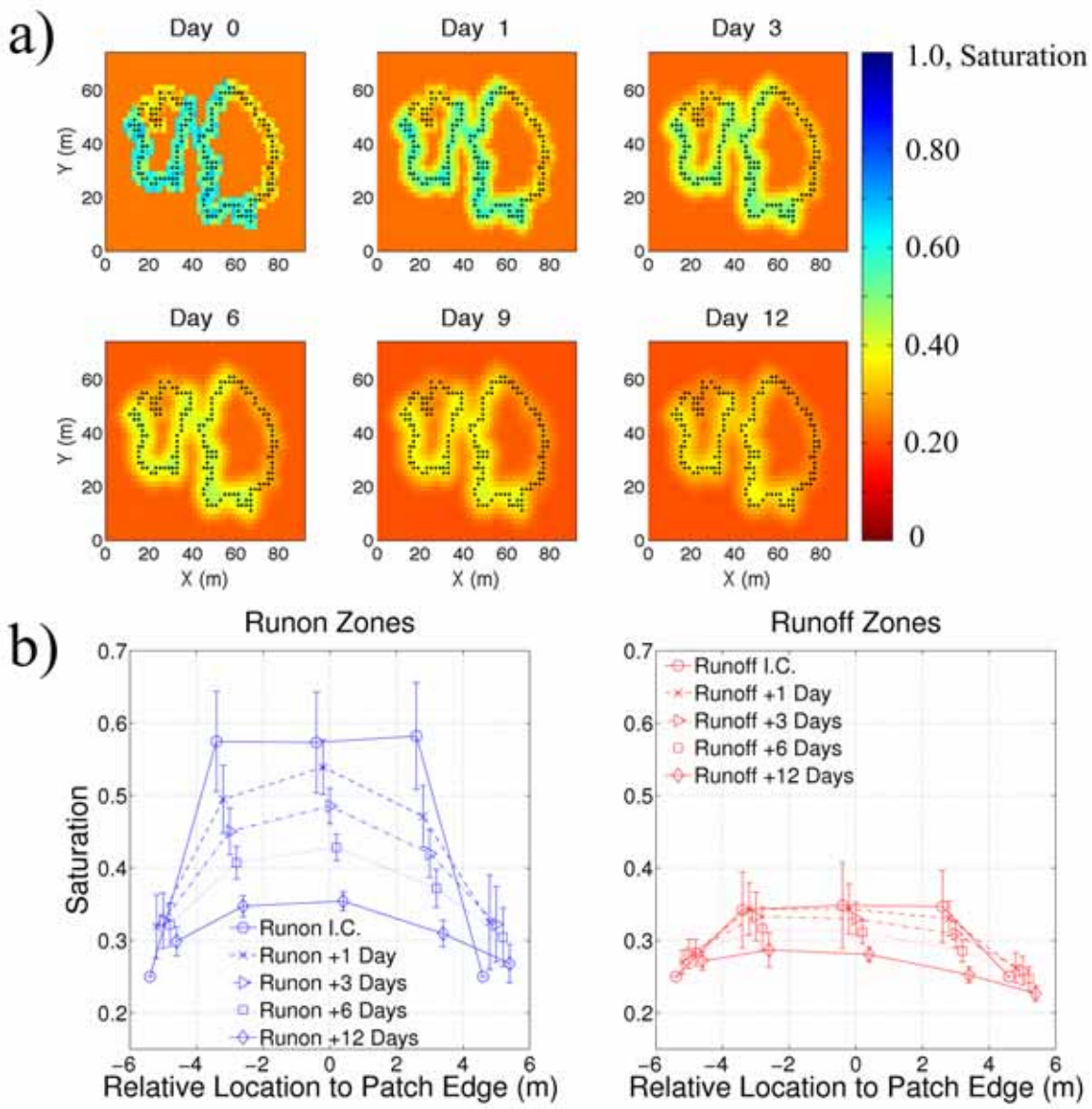

Figure 8. (a) A summary of the daily average saturations (the topsoil layer in the *XY* plane) from a quasi 3-dimensional numerical model using observed differences in initial saturations along patch boundaries from the April 2009 EMI data. (b) The changes of saturation (mean and ±1 SD) in time and around the patch perimeter (negative values are inside the patch) illustrate the affects of the localized vertical infiltration and horizontal redistribution of subsurface water. Note that the symbol locations along the *x* axis in Figure 8b were offset to clearly distinguish the different symbols.

[*Rodriguez-Iturbe and Porporato*, 2004]. Figure 3 suggests that the two tree species are clustered in two pockets around the different soil depth pools. Clustering of different tree species on the scale of tens to hundreds of meters is prevalent on hillslopes around the study area. The spatial organization of woody canopies occurs over a trees' lifetime and over many generations, integrating the outcomes of reproduction, establishment, growth, and survival, which can all be influenced by local resource conditions [*Scholes and Archer*, 1997]. While the timescale of the processes makes experimental studies impractical, through basic vegetation mapping and geophysical imaging we inferred an environmental variable associated with woody vegetation organization in this ecosystem.

[45] Given the dry, hard compacted sandy clay loam soils, it was not possible to hand auger to soil depths greater than 50 cm at this site in order to fully ground truth the modeled soil depths. In addition, access to heavy machinery at this remote location is limited; leaving only labor-intensive hand-excavated soil pits. However, the correlation between rock outcrops, shallow auger samples, and the simple geophysical model are promising. More vertical soundings followed by soil excavation pits to the bedrock would help resolve more of the uncertainty in the geophysical models at the Narok site. In addition, a more rigorous hydrogeophysical inversion analysis [*Auken et al.*, 2005; *Christiansen et al.*, 2007; *Siemon et al.*, 2009; *Viezzoli et al.*, 2008] may provide higher quality data by avoiding the homogeneous

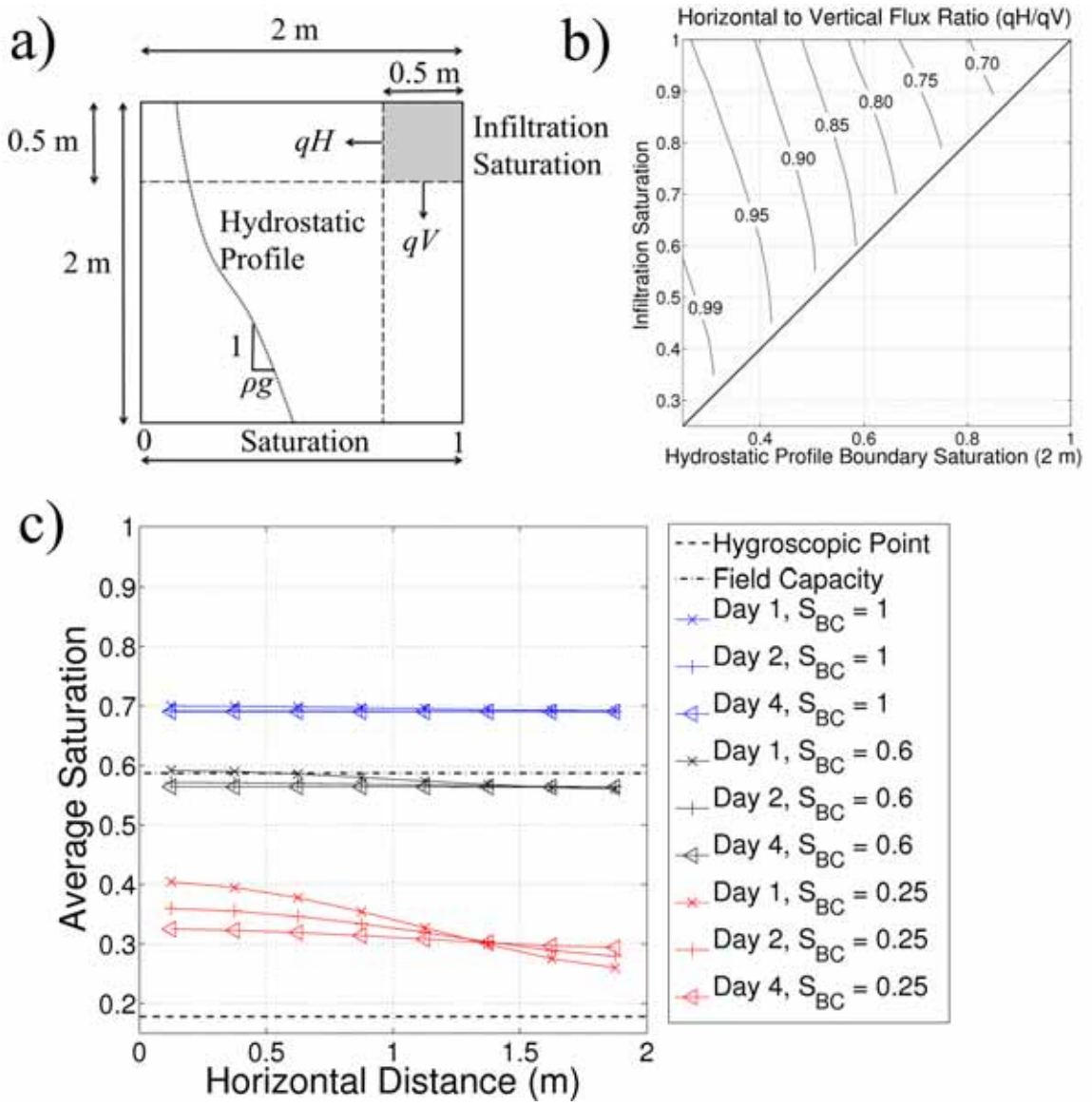

Figure 9. (a) The idealized domain and initial conditions of 2-dimensional *XZ*-plane modeling experiment representing preferential vertical infiltration around an *S. volkensii* patch margin. (b) The ratio of horizontal and vertical redistribution of subsurface water depends on the infiltration event saturation and the initial hydrostatic saturation profile (defined by saturation at the 2 m boundary). (c) The horizontal distance of redistributed water is dependent on the initial saturation profile in the domain, with drier conditions leading to longer horizontal redistribution. Note that the infiltration saturation was 1 for the results shown in Figure 9c.

earth assumption [*McNeill*, 1980], and including the spatial correlation directly in the inversion procedure as opposed to a geostatistical model used to smooth the data.

4.2. Mechanisms Controlling Herbaceous Layer Vegetation Dynamics

[46] The response of herbaceous layer vegetation to precipitation inputs occurs on the timescale of days to weeks in dryland ecosystems [*Scanlon et al.*, 2005]. The rapid response of grass has been shown to be an important resource-conserving buffer (i.e., water and sediment) of functioning savanna ecosystems [*Scanlon et al.*, 2007]. If this buffer is removed by intensive grazing, the hydrology of the system is altered, leading to increased surface runoff and decreased infiltration [*Kefi et al.*, 2007]. When combined with topography, the new rainfall-runoff-run on regime can lead to leaky landscapes [*Ludwig et al.*, 2007] and opportunities for unpredictable system changes due to nonlinearities and feedbacks [*Newman et al.*, 2006; *Turnbull et al.*, 2008]. Using time-lapse geophysical differencing techniques at the Nolkopin site, we identified a positive feedback mechanism that may have led to the recent proliferation of the undesirable succulent *S. volkensii* in central Kenya.

[47] An accepted positive feedback in dryland systems is that increased grazing intensity will lead to lower amounts of forage, which reduces water infiltration due to

the expansion of bare soil areas, which causes even greater loss of forage [*Whisenant*, 1999]. As with the heavily grazed Nolkopin site, our EMI observations (Figures 6 and 7) illustrated that more water infiltrated in vegetation patch run on versus runoff zones and inside patches versus outside patches. Furthermore, vegetation studies conducted around these patches, reported elsewhere, indicated *S. volkensii* was healthier and preferentially grew in run on versus runoff zones [*King et al.*, 2010]. Together, the observed vegetation and soil moisture dynamics suggest that surface water flows are driving the feedbacks that generate patterns of landscape heterogeneity, as is typical of degraded dryland ecosystem functioning [*Rietkerk et al.*, 2002, 2004].

[48] When the two sets of EMI imagery and continuous soil moisture monitoring of nine distinct rain events over a 16 month period (Figure 4) are considered together, the data suggest three distinct infiltration regimes, which are related to the concept of preferred states in spatial soil moisture patterns. The original concept of preferred states in spatial soil moisture patterns was developed for catchment scales and used to explain local and nonlocal controls of horizontal and vertical redistribution of water [*Grayson et al.*, 1997]. Here we expand on the preferred states of soil moisture to include a third state that is relevant for this patch–interpatch scale. Given the compacted nature of soils in this dryland ecosystem, Hortonian overland flow has been observed to begin with as little as 4–6 mm of rainfall on bare soil plots (Franz et al., submitted manuscript, 2011), leading to significant redistribution of surface water. The EMI observations and CS616 responses suggest three different infiltration regimes that control the horizontal and vertical redistribution of subsurface water. Small rainfall events (depth $<$5–10 mm, i.e., July 2009), result in some localized vertical infiltration in surface patch run on zones with minimal horizontal redistribution of subsurface water. Medium rainfall events (10$<$ depth $<$20–30 mm, i.e., May 2008, April 2009, and June 2009), result in greater localized vertical infiltration that is preferentially distributed in run on zones, leading to significant horizontal redistribution of subsurface water. This localized vertical infiltration and subsequent horizontal redistribution of subsurface water results in a "halo" of increased saturations in the topsoil zone around patches (Figures 7a–7e and 8a). Large rainfall events (depth $>$30 mm, i.e., June 2008, September 2008, and October 2008), result in widespread vertical infiltration around patches due to large rainfall totals and substantial run on from upstream bare areas. Some horizontal redistribution of subsurface waters may occur as conditions dry out at different rates in different patch types.

[49] The horizontal redistribution of subsurface water in medium and large rainfall events may catalyze a positive feedback that promotes the expansion of *S. volkensii* patches. In the "halo" outside the patch margins, the surface of the soil tends to be bare, compacted, and sealed due to the loss of perennial grass cover, which inhibits grass establishment because their roots cannot penetrate the soil [*King and Stanton*, 2008]. The hard soil surface does not, however, inhibit *S. volkensii* reproduction. The plant spreads by strong, 2 cm thick rhizomes that bore through the compacted soil beyond patch margins, and would then have sole access to the below groundwater resource pool in the outer halo (E. G. King et al., Ecohydrological interactions in a degraded two-phase mosaic dryland: implications for regime shifts, resilience, and restoration, submitted to *Ecohydrology*, 2011). The proliferation of *S. volkensii* after rangeland degradation may therefore be due to the positive feedback generated as *S. volkensii* patches repeatedly induce the formation of a soil moisture "halo" beyond their margin after medium and large rain events, which they can then expand into and utilize. An analysis of historical daily rainfall patterns in the basin indicated that total annual rainfall has remained constant but the intensity and time between rainfall events are increasing with time [*Franz et al.*, 2010], which will likely lead to an increased frequency in the medium infiltration regime and redistribution patterns. We note that our discussion is primarily focused on daily rainfall depth, but changes in the intensity of individual storm events may have similar consequences and we refer the reader to Franz et al. (submitted manuscript, 2011) for a discussion of storm intensity and impacts on this ecosystem. The time-lapse EMI study at Nolkopin and numerical modeling have yielded significant insights into the feedbacks between resource heterogeneity and vegetation organization. The role of positive feedbacks and rainfall dependency in promoting the spread of *S. volkensii* also have important implications for the future trajectory of ecosystem change and the options for managing land degradation.

5. Conclusions

[50] Understanding the complex patterns and processes occurring in natural ecosystems requires innovative technologies and experimental designs. However, the use of indirect methods, such as EMI, requires careful interpretation of the complex data. In order to address such issues, we used a suite of measurements, soil laboratory testing, geophysical models, and a numerical model to validate and understand the measurements. The EMI measurements were central to our multidisciplinary approach for linking geophysical, hydrological, and vegetation dynamics in each of the case studies (Figure 1). At Narok, it allowed us to identify resource conditions influencing the spatial clustering of woody vegetation, and at Nolkopin it was essential in elucidating the patterns and mechanisms of soil moisture redistribution, as well as feedbacks that may be responsible for the proliferation of *S. volkensii.* The nondestructive nature and the high degree of spatial and temporal resolution attainable for the sampling effort make EMI an increasingly valuable tool for integrative research on landscape function. Its future utility will grow as coupled hydrogeophysical inversion methods continue to be explored and refined.

[51] **Acknowledgments.** The authors would like to thank the Mpala Research Centre, Koija Group Ranch, A. Lekutaas, and T. Lolkirik for onsite support in Kenya. K. K. Caylor and T. E. Franz would like to thank NSF OISE-0854708, NSF CAREER award to K. Caylor EAR-847368, and Princeton University funding sources including: Grand Challenges, the Walbridge Fellowship, and the Technology for Developing Regions Fellowship for their financial support. We would also like to thank three anonymous reviewers for their helpful comments.

References

Abdu, H., D. A. Robinson, and S. B. Jones (2007), Comparing bulk soil electrical conductivity determination using the DUALEM-1S and EM38-DD electromagnetic induction instruments, *Soil Sci. Soc. Am. J.*, *71*(1), 189–196.

Abdu, H., D. A. Robinson, M. Seyfried, and S. B. Jones (2008), Geophysical imaging of watershed subsurface patterns and prediction of soil

texture and water holding capacity, *Water Resour. Res.*, *44*, W00D18, doi:10.1029/2008wr007043.

Asbjornsen, H., et al. (2011), Ecohydrological advances and applications in plant-water relations research: A review, *J. Plant Ecol.*, *4*(1–2), 3–22, doi:10.1093/jpe/rtr005.

Auken, E., A. V. Christiansen, B. H. Jacobsen, N. Foged, and K. I. Sorensen (2005), Piecewise 1D laterally constrained inversion of resistivity data, *Geophys. Prospect.*, *53*(4), 497–506.

Belnap, J., and D. A. Gillette (1998), Vulnerability of desert biological soil crusts to wind erosion: the influences of crust development, soil texture, and disturbance, *J. Arid Environ.*, *39*(2), 133–142.

Belsky, A. J., R. G. Amundson, J. M. Duxbury, S. J. Riha, A. R. Ali, and S. M. Mwonga (1989), The effects of trees on their physical, chemical, and biological environments in a semi-arid savanna in Kenya, *J. Appl. Ecol.*, *26*(3), 1005–1024.

Bond, W. J. (2008), What limits trees in C-4 grasslands and savannas?, *Annu. Rev. Ecol. Evol. Syst.*, *39*, 641–659, doi:10.1146/annurev.ecolsys.110707.173411.

Borgogno, F., P. D'Odorico, F. Laio, and L. Ridolfi (2009), Mathematical models of vegetation pattern formation in ecohydrology, *Rev. Geophys.*, *47*, RG1005, doi:10.1029/2007rg000256.

Breshears, D. D., O. B. Myers, and F. J. Barnes (2009), Horizontal heterogeneity in the frequency of plant-available water with woodland intercanopy-canopy vegetation patch type rivals that occuring vertically by soil depth, *Ecohydrology*, *2*(4), 503–519. doi:10.1002/eco.75.

Brody, A. K., T. M. Palmer, K. Fox-Dobbs, and D. F. Doak (2010), Termites, vertebrate herbivores, and the fruiting success of acacia drepanolobium, *Ecology*, *91*, 399–407.

Christiansen, A. V., E. Auken, N. Foged, and K. I. Sorensen (2007), Mutually and laterally constrained inversion of CVES and TEM data: A case study, *Near Surf. Geophys.*, *5*(2), 115–123.

Darlington, J. (1997), Comparison of nest structure and caste parameters of sympatric species of Odontotermes (Termitidae, Macrotermitinae) in Kenya, *Insectes Sociaux*, *44*(4), 393–408.

Darlington, J. (2005), Termite nest structure and impact on the soil at the radar site, Embakasi, Kenya (Isoptera: Termitidae), *Sociobiology*, *45*(3), 521–542.

Dharani, N. (2006), *Field Guide to Acacias of East Africa*, 200 pp., Struik Publ., Cape Town, Africa.

Doolittle, J. A., K. A. Sudduth, N. R. Kitchen, and S. J. Indorante (1994), Estimating depths to claypans using electromagnetic induction methods, *J. Soil Water Conserv.*, *49*(6), 572–575.

Ferré, T., L. Bentley, A. Binley, N. Linde, A. Kemna, K. Singha, K. Holliger, J. A. Huisman, and B. Minsley (2009), Critical steps for the continuing advancement of hydrogeophysics, *Eos Trans. AGU*, *90*(23), 200, doi:10.1029/2009EO230004.

Fox-Dobbs, K., D. F. Doak, A. K. Brody, and T. M. Palmer, (2010), Termites create spatial structure and govern ecosystem function by affecting n-2 fixation in an East African savanna, *Ecology*, *91*, 1296–1307.

Franz, T. E., K. K. Caylor, J. M. Nordbotten, R. I. Rodriguez-Iturbe, and M. A. Celia (2010), An ecohydrological approach to predicting regional woody species distribution patterns in dryland ecosystems, *Adv. Water Resour.*, *33*, 215–230, doi:10.1016/j.advwatres.2009.12.003.

Franz, T. E., J. Nolan, J. M. Nordbotten, K. K. Caylor, and L. D. Slater (2011), Quantifying transient soil moisture dynamics using multipoint direct-current resistivity in homogeneous sand, *Vadose Zone J.*, *10*(1), 286–298, doi:10.2136/vzj2010.0031.

Fratkin, E. (1997), Pastoralism: Governance and development issues, *Ann. Rev. Anthropology*, *26*, 235–261.

Fratkin, E., and R. Mearns (2003), Sustainability and pastoral livelihoods: Lessons from East African Maasai and Mongolia, *Human Organization*, *62*(2), 112–122.

Fratkin, E., E. A. Roth, and M. A. Nathan (2004), Pastoral sedentarization and its effects on children's diet, health, and growth among Rendille of northern Kenya, *Human Ecology*, *32*(5), 531–559.

Gebrehiwot, K., B. Muys, M. Haile, and R. Mitloehner (2005), The use of plant water relations to characterize tree species and sites in the drylands of northern Ethiopia, *J. Arid Environ.*, *60*(4), 581–592.

Goovaerts, P. (1997), *Geostatistics for Natural Resources Evaluation*, 512 pp., Oxford Univ. Press, New York.

Grayson, R. B., A. W. Western, F. H. S. Chiew, and G. Bloschl (1997), Preferred states in spatial soil moisture patterns: Local and nonlocal controls, *Water Resour. Res.*, *33*(12), 2897–2908, doi:10.1029/97WR02174.

Hendrickx, J. M. H., and R. G. Kachanoski (2002), Nonintrusive electromagnetic induction, in *Methods of Soil Analysis*, Part 1, edited by J. Dane and C. Topp, pp. 1301–1310, Soil Sci. Soc. of Am., Madison, WI.

Higgins, S. I., et al. (2007), Effects of four decades of fire manipulation on woody vegetation structure in savanna, *Ecology*, *88*(5), 1119–1125.

Hinnell, A. C., T. P. A. Ferré, J. A. Vrugt, J. A. Huisman, S. Moysey, J. Rings, and M. B. Kowalsky (2010), Improved extraction of hydrologic information from geophysical data through coupled hydrogeophysical inversion, *Water Resour. Res.*, *46*, W00D40, doi:10.1029/2008WR007060.

Jones, S. B., J. M. Blonquist, D. A. Robinson, V. P. Rasmussen, and D. Or (2005), Standardizing characterization of electromagnetic water content sensors: Part 1. Methodology, *Vadose Zone J.*, *4*(4), 1048–1058.

Kachanoski, R. G., and E. Dejong (1988), Scale dependence and the temporal persistence of spatial patterns of soil-water storage, *Water Resour. Res.*, *24*(1), 85–91, doi:10.1029/WR024i001p00085.

Kefi, S., M. Rietkerk, C. L. Alados, Y. Pueyo, V. P. Papanastasis, A. ElAich, and P. C. de Ruiter (2007), Spatial vegetation patterns and imminent desertification in Mediterranean arid ecosystems, *Nature*, *449*(7159), 213–U215, doi:10.1038/nature06111.

Kelleners, T. J., M. S. Seyfried, J. M. Blonquist, J. Bilskie, and D. G. Chandler (2005), Improved interpretation of water content reflectometer measurements in soils, *Soil Sci. Soc. Am. J.*, *69*(6), 1684–1690.

King, E. G., and M. L. Stanton (2008), Facilitative effects of *Aloe* shrubs on grass establishment, growth, and reproduction in degraded Kenyan rangelands: Implications for restoration, *Restoration Ecology*, *16*(3), 464–474. doi:10.1111/j.1526-100X.2007.00310.x.

King, E. G., T. E. Franz, and K. K. Caylor (2010), Proliferation of a Native Succulent in Kenyan Drylands: Ecohydrology and Resilience, paper presented at Ecological Society of America, Pittsburgh, PA, August 5, 2010.

Kiome, R., and M. Stocking (1993), Soil and Water Conservation in Semi-arid Kenya, Natural Resource Institute Bulletin 61, 59 pp., Chatham, U. K.

Lee, B. D., B. J. Carter, P. A. Ward, R. S. Taylor, and L. P. Lee (2004), Morphology of mounded soils in the Ouachita physiographic province, eastern Oklahoma, paper presented at ASA, Madison, WI.

Lehmann, P., S. Assouline, and D. Or (2008), Characteristic lengths affecting evaporative drying of porous media, *Phys. Rev. E*, *77*(5), 16, doi:05630910.1103/PhysRevE.77.056309.

Lin, H., J. Bouma, Y. Pachepsky, A. Western, J. Thompson, R. van Genuchten, H. J. Vogel, and A. Lilly (2006), Hydropedology: Synergistic integration of pedology and hydrology, *Water Resour. Res.*, *42*, W05301 doi:10.1029/2005wr004085.

Ludwig, F., T. E. Dawson, H. Kroon, F. Berendse, and H. H. T. Prins (2003), Hydraulic lift in Acacia tortilis trees on an East African savanna, *Oecologia*, *134*(3), 293–300.

Ludwig, J. A., B. P. Wilcox, D. D. Breshears, D. J. Tongway, and A. C. Imeson (2005), Vegetation patches and runoff-erosion as interacting ecohydrological processes in semiarid landscapes, *Ecology*, *86*(2), 288–297.

Ludwig, J. A., G. N. Bastin, V. H. Chewings, R. W. Eager, and A. C. Liedloff (2007), Leakiness: A new index for monitoring the health of arid and semiarid landscapes using remotely sensed vegetation cover and elevation data, *Ecol. Indicators*, *7*(2), 442–454. doi:10.1016/j.ecolind.2006.05.001.

McNeill, J. D. (1980), Electromagnetic terrain conductivity measurement at low induction numbers. Technical Note TN-6, edited.

Mwangi, E. (2007), The puzzle of group ranch subdivision in Kenya's Maasailand, *Dev. Change*, *38*(5), 889–910.

Newman, B. D., B. P. Wilcox, S. R. Archer, D. D. Breshears, C. N. Dahm, C. J. Duffy, N. G. McDowell, F. M. Phillips, B. R. Scanlon, and E. R. Vivoni (2006), Ecohydrology of water-limited environments: A scientific vision, *Water Resour. Res.*, *42*, W06302, doi:10.1029/2005wr004141.

Njenga, M. (2001), Community based natural resource management (CBNRM) participatory rural appraisal, Koija NRM (Group Ranch), Semi Arid Rural Development Programme (SARDEP)—Laikipia, Nanyuki, Kenya.

Palmer, T. M. (2003), Spatial habitat heterogeneity influences competition and coexistence in an African acacia ant guild, *Ecology*, *84*(11), 2843–2855.

Pinder, G. F., and M. A. Celia (2006), *Subsurface Hydrology*, 468 pp., John Wiley & Sons, Hoboken, N. J.

Pringle, R. M., D. F. Doak, A. K. Brody, R. Jocque, and T. M. Palmer (2010), Spatial pattern enhances ecosystem functioning in an African savanna, *PLoS Biol.*, *8*(5), e1000377, doi:10.1371/journal.pbio.1000377.

Remy, N. (2005), The Stanford geostatistical modeling software: A tool for new algorithms development, in *Geostatistics Banff* 2004, edited by O. Leuangthong and C. V. Deutsch, pp. 865–871, Springer, New York.

Rietkerk, M., M. C. Boerlijst, F. van Langevelde, R. HilleRisLambers, J. van de Koppel, L. Kumar, H. H. T. Prins, and A. M. de Roos (2002), Self-organization of vegetation in arid ecosystems, *Am. Naturalist*, *160*(4), 524–530.

Rietkerk, M., S. C. Dekker, P. C. de Ruiter, and J. van de Koppel. (2004), Self-organized patchiness and catastrophic shifts in ecosystems, *Science*, *305*(5692), 1926–1929.

Robinson, D. A., H. Abdu, S. B. Jones, M. Seyfried, I. Lebron, and R. Knight (2008a), Eco-geophysical imaging of watershed-scale soil patterns links with plant community spatial patterns, *Vadose Zone J.*, *7*(4), 1132–1138, doi:10.2136/vzj2008.0101.

Robinson, D. A., C. S. Campbell, J. W. Hopmans, B. K. Hornbuckle, S. B. Jones, R. Knight, F. Ogden, J. Selker, and O. Wendroth (2008b), Soil moisture measurement for ecological and hydrological watershed-scale observatories: A review, *Vadose Zone J.*, *7*(1), 358–389.

Robinson, D. A., I. Lebron, B. Kocar, K. Phan, M. Sampson, N. Crook, and S. Fendorf (2009), Time-lapse geophysical imaging of soil moisture dynamics in tropical deltaic soils: An aid to interpreting hydrological and geochemical processes, *Water Resour. Res.*, *45*, W00D32, doi:10.1029/2008wr006984.

Rodriguez-Iturbe, I., and A. Porporato (2004), *Ecohydrology of Water-Controlled Ecosystems*, 442 pp., Cambridge Univ. Press, New York.

Sankaran, M., et al. (2005), Determinants of woody cover in African savannas, *Nature*, *438*(7069), 846–849.

Sankaran, M., J. Ratnam, and N. Hanan (2008), Woody cover in African savannas: The role of resources, fire and herbivory, *Global Ecol. Biogeogr.*, *17*(2), 236–245, doi:10.1111/j.1466-8238.2007.00360.x.

Scanlon, T. M., K. K. Caylor, S. Manfreda, S. A. Levin, and I. Rodriguez-Iturbe (2005), Dynamic response of grass cover to rainfall variability: Implications for the function and persistence of savanna ecosystems, *Adv. Water Resour.*, *28*(3), 291–302, doi:10.1016/j.advwatres.2004.10.014.

Scanlon, T. M., K. K. Caylor, S. A. Levin, and I. Rodriguez-Iturbe (2007), Positive feedbacks promote power-law clustering of Kalahari vegetation, *Nature*, *449*(7159), 209–U204, doi:10.1038/nature06060.

Schaap, M. G., F. J. Leij, and M. T. van Genuchten (2001), ROSETTA: A computer program for estimating soil hydraulic parameters with hierarchical pedotransfer functions, *J. Hydrol.*, *251*(3–4), 163–176.

Scheffer, M., J. Bascompte, W. A. Brock, V. Brovkin, S. R. Carpenter, V. Dakos, H. Held, E. H. van Nes, M. Rietkerk, and G. Sugihara (2009), Early-warning signals for critical transitions, *Nature*, *461*(7260), 53–59. doi:10.1038/nature08227.

Scholes, R. J., and S. R. Archer (1997), Tree-grass interactions in savannas, *Ann. Rev.Ecol. System.*, *28*, 517–544.

Sheets, K. R., and J. M. H. Hendrickx (1995), Noninvasive soil-water content measurement using electromagnetic induction, *Water Resour. Res.*, *31*(10), 2401–2409.

Sherlock, M. D., and J. J. McDonnell (2003), A new tool for hillslope hydrologists: Spatially distributed groundwater level and soilwater content measured using electromagnetic induction, *Hydrol. Processes*, *17*(10), 1965–1977, doi:10.1002/hyp.1221.

Shokri, N., P. Lehmann, and D. Or (2009), Critical evaluation of enhancement factors for vapor transport through unsaturated porous media, *Water Resour. Res.*, *45*, W10433, doi:10.1029/2009wr007769.

Siemon, B., E. Auken, and A. V. Christiansen (2009), Laterally constrained inversion of helicopter-borne frequency-domain electromagnetic data, *J. Appl. Geophys.*, *67*(3), 259–268. doi:10.1016/j.jappgeo.2007.11.003.

Simunek, J., M. T. van Genuchten, and M. Sejna (2006), The HYDRUS Software Package for Simulating the Two- and Three-Dimensional Movement of Water, Heat, and Multiple Solutes in Variably-Saturated Media, Technical Manual, Version 1.0.

Tietjen, B., F. Jeltsch, E. Zehe, N. Classen, A. Groengroeft, K. Schiffers, and J. Oldeland (2010), Effects of climate change on the coupled dynamics of water and vegetation in drylands, *Ecohydrology*, *3*(2), 226–237, doi:10.1002/eco.70.

Triantafilis, J., and S. M. Lesch (2005), Mapping clay content variation using electromagnetic induction techniques, *Comput. Electron. Agri.*, *46*(1–3), 203–237, doi:10.1016/j.compag.2004.11.006.

Triantafilis, J., I. O. A. Odeh, and A. B. McBratney (2001), Five geostatistical models to predict soil salinity from electromagnetic induction data across irrigated cotton, *Soil Sci. Soc. Am. J.*, *65*(3), 869–878.

Turnbull, L., J. Wainwright, and R. E. Brazier (2008), A conceptual framework for understanding semi-arid land degradation: Ecohydrological interactions across multiple-space and time scales, *Ecohydrology*, *1*(1), 23–34, doi:10.1002/eco.4.

Turner, J. S. (2006), Termites as mediators of the water economy of arid savanna ecosystems, in *Dryland Ecohydrology*, edited by P. D'Odorico and A. Porporato, pp. 303–313, Springer, Dordrecht, Netherlands.

Vangenuchten, M. T. (1980), A closed-form equation for predicting the hydraulic conductivity of unsaturated soils, *Soil Sci. Soc. Am. J.*, *44*(5), 892–898.

Vereecken, H., J. A. Huisman, H. Bogena, J. Vanderborght, J. A. Vrugt, and J. W. Hopmans (2008), On the value of soil moisture measurements in vadose zone hydrology: A review, *Water Resour. Res.*, *44*, W00D06, doi:10.1029/2008wr006829.

Viezzoli, A., A. V. Christiansen, E. Auken, and K. Sorensen (2008), Quasi-3D modeling of airborne TEM data by spatially constrained inversion, *Geophysics*, *73*(3), F105–F113, doi:10.1190/1.2895521.

Walpole, R. E., R. H. Myers, S. L. Myers, and K. Ye (2002), *Probability and Statistics for Engineers and Scientists*, 7th ed., 816 pp., Prentice Hall, Upper Saddle River, N. J.

Whisenant, S. G. (1999), *Repairing Damaged Wildlands: A Process-Oriented, Landscape-Scale Approach*, 312 pp., Cambridge Univ. Press, New York.

Young, T. P., N. Patridge, and A. Macrae (1995), Long-term glades in acacia bushland and their edge effects in Laikipia, Kenya, *Ecol. Appl.*, *5*(1), 97–108.

Young, T. P., B. Okello, D. Kinyua, and T. M. Palmer (1998), KLEE: A long-term multi-species herbivore exclusion experiment in Laikipia, Kenya, *African Journal of Range & Forage Science*, *14*, 92–104.

K. K. Caylor and T. E. Franz, Department of Civil and Environmental Engineering, Princeton University, E209a Engineering Quad, Princeton, NJ 08544, USA. (tfranz@princeton.edu)

E. G. King, Department of Ecology and Evolutionary Biology, Princeton University, Guyot Hall, Rm. 106, Princeton, NJ 08544, USA.

D. A. Robinson, Centre for Ecology and Hydrology, Environment Centre Wales, Deiniol Road, Bangor LL57 2UW, UK.